NiTiHf High Temperature Shape Memory Alloy Design with the Assistance of Machine Learning

by

Aysel Aysu Çatal

A Dissertation Submitted to the
Graduate School of Sciences and Engineering
in Partial Fulfillment of the Requirements for
the Degree of

Master of Science

in

Mechanical Engineering

KOÇ ÜNİVERSİTESİ

January , 2022

NiTiHf High Temperature Shape Memory Alloy Design with the Assistance of Machine Learning

Koç University

Graduate School of Sciences and Engineering

This is to certify that I have examined this copy of a master's thesis by

Aysel Aysu Çatal

and have found that it is complete and satisfactory in all respects,

and that any and all revisions required by the final

examining committee have been made.

Committee Members:

Prof. Demircan Canadinç (Advisor)

Associate Prof. Ozan Kocadağlı

Assistant Prof. Mine Toker

Date: 03.01.2022________________________

Dedicated to my family

ABSTRACT

NiTiHf High Temperature Shape Memory Alloy Design with the Assistance of Machine Learning

Aysel Aysu Çatal

Master of Science in Mechanical Engineering

January 3, 2022

The shape memory alloys demonstrate a unique property that allows them to recover enormous shape changes above certain temperatures; therefore, they are a notable option as a compliant actuator. Increasing demand in the aerospace and oil industry for high-temperature actuators motivates the search for high-temperature shape memory alloys. High operating temperature range, medium-ductility, and remarkably lower cost of NiTiHf alloys distinguish them from various high-temperature shape memory alloy systems. However, as a ternary alloy system, NiTiHf alloys have vast search space to be analyzed, which requires significant investment. On the other hand, the implementation of machine learning in material science has been proven promising and affordable alternative for experimental search, which gave inspiration to current work: designing NiTiHf shape memory alloy that can exhibit phase transformation beyond 400 ℃ with the assistance of machine learning.

In this work, a comprehensive dataset was established from the available literature on NiTiHf alloy for training by a multilayer feedforward neural network algorithm. Via the optimized neural network model, phase transformation temperatures of unexplored NiTiHf search space were estimated. Two novel compositions with desired functions, namely the $Ni_{49.7}Ti_{26.6}Hf_{23.7}$, and the $Ni_{50}Ti_{27}Hf_{23}$ alloys, were selected to validate machine learning predictions. The former demonstrated an A_f temperature of 403.5 °C with high cyclic stability, which verifies the success of machine learning in new alloy design.

ÖZETÇE

Makine Öğreniminin Yardımıyla Yüksek Sıcaklıkta NiTiHf Şekil Hafızalı Alaşım Tasarımı

Aysel Aysu Çatal
Makine Mühendisliği, Yüksek Lisans
3 Ocak 2022

Şekil hafızalı alaşımlar, belirli sıcaklıkların üzerinde şekil değişikliklerini telafi etmelerine izin veren benzersiz bir özellik sergiler; bu nedenle uyumlu bir aktüatör olarak dikkate değer bir seçenektir. Havacılık ve petrol endüstrisinde yüksek sıcaklıklı aktüatörlere yönelik artan talep, yüksek sıcaklıkta şekil hafızalı alaşımlar arayışını motive etmektedir. NiTiHf alaşımlarının yüksek çalışma sıcaklığı aralığı, orta süneklik ve dikkate değer ölçüde düşük maliyeti, onları çeşitli yüksek sıcaklık şekil hafızalı alaşım sistemlerinden ayırır. Bununla birlikte, üçlü bir alaşım sistemi olarak NiTiHf alaşımları, analizi önemli yatırımlar gerektiren geniş bir arama alanına sahiptir. Öte yandan, malzeme biliminde makine öğreniminin uygulanmasının deneysel araştırmalara umut verici ve uygun fiyatlı bir alternatif olduğu kanıtlanmış ve mevcut çalışmaya ilham vermiştir: makine öğrenimi yardımıyla 400 °C ötesinde faz dönüşümü gösterebilen NiTiHf şekil hafızalı alaşım tasarlama.

Bu çalışmada, NiTiHf alaşımı ile ilgili mevcut literatürden bir veri seti oluşturulmuştur. Hazırlanan veri setini eğitmek için çok katmanlı ileri beslemeli bir sinir ağı oluşturulmuştur. İlgili fiziksel özellikler belirlenmiş ve optimal özellik setini seçmek için sarmalama metodolojisi kullanılmıltır. Sinir ağı modeli, deneme yanılma yoluyla düğüm sayısı ve düzenlileştirme parametreleri ayarlanarak optimize edilmiştir. $Ni_{49.7}Ti_{26.6}Hf_{23.7}$ ve $Ni_{50}Ti_{27}Hf_{23}$ alaşımları olmak üzere istenen işlevlere sahip iki bileşim, makine öğrenimi tahminlerini doğrulamak için seçildi. $Ni_{49.7}Ti_{26.6}Hf_{23.7}$ alaşımı, yüksek döngüsel kararlılıkla 403.5 °C 'lik bir A_f sıcaklığı gösterdi.

ACKNOWLEDGMENTS

First and foremost, I would like to thank my advisor, Prof. Demircan Canadinç, for the opportunity of participating in his group. Over the last two years, he continued to support, guide, and assist me throughout pursuing the M.Sc. degree. The things I learned from him will be invaluable all through my life and, hopefully, one day, I will be a mentor just like him. I would also like to thank the thesis committee members, Dr. Ozan Kocadağlı and Dr. S. Mine Toker, for their participation and interest. I am glad to have the chance to get their suggestions and comments on my thesis.

I should show my gratitude to TUSAŞ Engine Industries, particularly my colleague Elif Bedir and Rıfat Yılmaz; this project would not be successful without their help. Additionally, I am grateful for the scientific environment Koç University provided, which allowed me to get benefit from the knowledge of Dr. Hadi Jahangiri, Dr. Amir Motallebzadeh, and Dr. Barış Yağcı. I feel very fortunate to have the companionship of my friends in the Advanced Materials Group, Alireza, İbrahim, Shabnam, Can, and Azizeh. Surrounding these intelligent and amusing people motivated me a lot.

I appreciate my parents Nurşen and Veysel Çatal, and my siblings Cansu and Vugar, since I know that they are here for me all the time. Lastly, I am thankful to Mert Işık for his unconditional support and understanding.

TABLE OF CONTENTS

LIST OF TABLES

LIST OF FIGURES

ABBREVIATIONS

ANN	Artificial Neural Network
A_f	Austenite Finish Temperature
A_s	Austenite Start Temperature
DSC	Differential Scanning Calorimetry
EDM	Electrical Discharge Machining
ε_{irr}	Irrecoverable Strain
ε_{rec}	Recoverable Strain
ε_{sme}	Shape Strain
HTSMA	High Temperature Shape Memory Alloys
M_f	Martensite Finish Temperature
M_s	Martensite Start Temperature
ML	Machine Learning
MLFFNN	Multi-Layer Feed Forward Neural Network
MSE	Mean Squared Error
MT	Martensitic Transformation
NN	Neural Network
R^2	Least Squared Parameter
RMSE	Root Mean Squared Error
RT	Reversible Phase Transformation
SMA	Shape Memory Alloy
SME	Shape Memory Effect
TT	Transformation Temperature

Chapter 1:
INTRODUCTION

1.1 Motivation

Currently, the demand for actuators that can operate at elevated temperatures is increasing in the aerospace industry. Even though the commercial actuators are dominated by hydraulic, pneumatic, or electric structures, these systems have several disadvantages, such as safety issues or energy loss due to friction, owing to their complexity. These drawbacks encouraged researchers to develop an alternative material that could eliminate the aforementioned disadvantages; hence, shape memory alloys were considered potential materials that could replace conventional complex structures. Besides their lower weights and relatively high-power capacities, as shown in Figure 1.1, shape memory alloys have a unique mechanism that allows them to actuate according to temperature change as a compliant mechanism. However, conventional shape memory alloys are restricted to applications below 100 °C; therefore, advancement in designing high-temperature shape memory alloys is required to supply the demand in the aerospace industry.

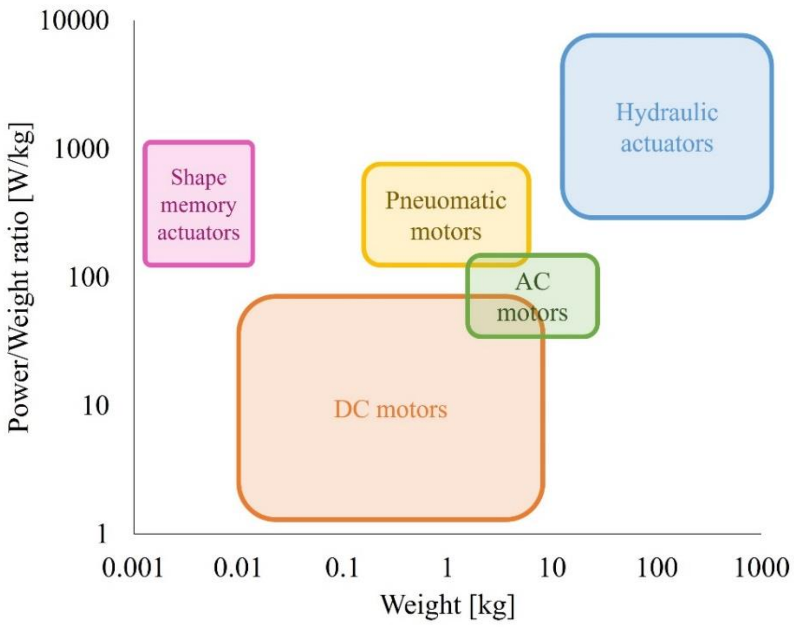

Figure 1.1. Power/weight ratio to the weight of shape memory alloys and commercial actuators [1]

Recent studies indicate that ternary alloying of NiTi with Pd, Pt, Au resulted in alloys that can operate at temperatures above 600 °C; nevertheless, the major drawback of these alloys was their expensiveness. Fortunately, NiTiHf shape memory alloys were regarded as a cost-effective candidate for elevated temperatures. Although the contributions of researchers among the last few decades disclosed more than 60 different NiTiHf compositions, there is still an enormous search space of NiTiHf unexplored yet. The discovery of a NiTiHf composition with higher operating temperatures and better shape memory properties, on the other hand, necessitates a detailed design of experimentations and a significant investment of time and resources. On the contrary, machine learning applications in material science may lead researchers to design optimal compositions without dealing with expensive experiments by predicting undiscovered alloys based on available literature. Consequently, in the current work, the implementation of machine learning technology on NiTiHf alloys was regarded as a promising design methodology, and validation experiments were conducted to assess its capability.

1.2 Background

This section supplies background information about shape memory alloys and machine learning. Notably, high-temperature shape memory alloys, their aspects, application areas, pros and cons, and the factors that affect shape memory properties are emphasized. Moreover, the feedforward multilayer neural network model is examined in detail. Finally, the implementations of a machine learning algorithm in material science are highlighted, and previous works focused on this field are interpreted.

1.2.1 Shape Memory Alloys

The discovery of shape memory alloys resulted from the contributions of numerous scientists in the 20th century. In 1949, Kurdjumov and Khandros [2] observed a thermoelastic martensitic transformation in CuZn and CuAl alloys and presented the phenomenon of reversible martensitic transformation. However, the main turning point was the introduction of NiTi (nitinol) by Buehler et al. in 1963, which stimulated engineering applications of SMAs [3]. The nitinol has attracted noticeable attention in the following years, and researchers focused on NiTi alloying with an additional element. Even though SMAs that can operate above 100 °C were developed in 1970 [4], the commercial applications were restricted to lower temperatures. Nevertheless, the demand for compliant actuators in the aerospace and oil industries encourages researchers to study NiTi-based ternary SMAs that can operate at elevated temperatures [5].

The shape memory effect (SME) is an exciting feature of alloys that can transform into their original shape above a specific temperature. The alloys that can exhibit SME are named shape memory alloys (SMAs), and the threshold temperature at which SMAs change into their initial form is called reverse transformation temperature. SMAs have two distinct phases: the parent phase (austenite) and martensite. The former can be observed at elevated temperatures and, generally, a simple cubic phase. On the other hand, martensite, in which the symmetry is lower than the parent phase, exists at low temperatures. The phase transformation from parent phase to martensite is known as martensitic transformation (MT), which is a diffusionless solid to solid transformation related to the ability of SMAs to remember their shape. A simple model of MT is illustrated in Figure 1.2, in which the two different variants of martensite and parent phase are indicated [6,7].

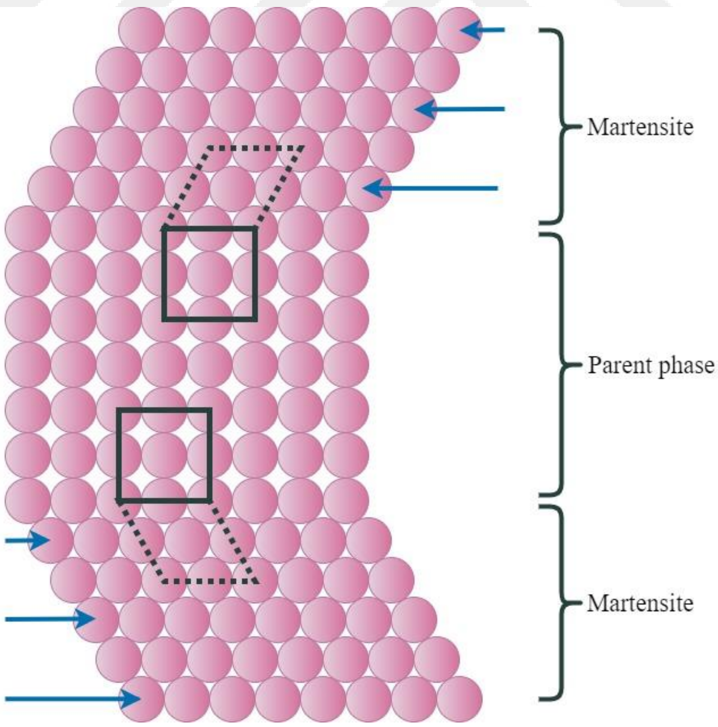

Figure 1.2. Illustration of martensitic transformation [6]

MT in SMAs has a distinguishable property called reversible phase transformation (RT) that prevents large strain by creating twinned martensite structures. Twinned martensite is also called self-accommodated martensite due to its ability to accommodate excessive strain. The single variant, in other words, detwinned martensite appears if stress is applied on twinned martensite; however, when the material is heated up and cooled down, the original twinned martensite is formed due to the nature of RT. This cycle is demonstrated in Figure 1.3 [8,9].

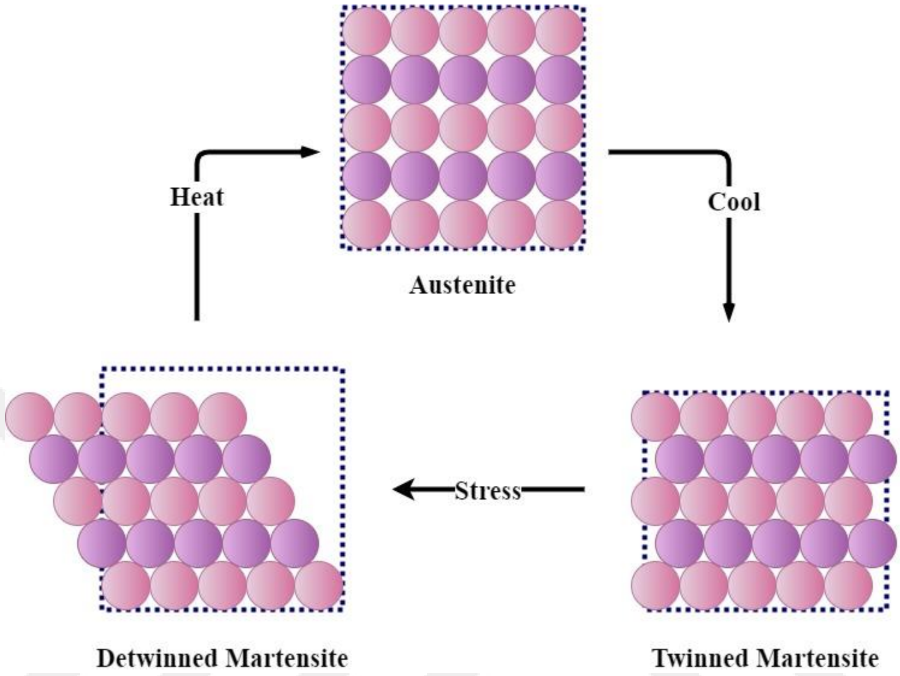

Figure 1.3. Demonstration of martensite and austenite structures [9]

Compared to Figure 1.3, SMAs exhibit MT and RT more convolutedly. Transformations happen gradually between certain temperatures, which are namely martensite start (M_s), martensite finish (M_f), austenite start (A_s), and austenite finish (A_f) temperatures, respectively. These temperatures, indicated on the thermal cycle graph given in Figure 1.4, depend on a number of factors such as the applied load, chemical composition, and microstructure, which will be discussed in detail later.

Another unique property of SMAs is pseudoelasticity which is also known as superelasticity. Pseudoelasticity is the ability of SMAs to recover a significant amount of strain by the removal of applied force at elevated temperatures. It can be observed at temperatures above $A_{f,}$ and the phase transformation occurs between austenite (absence of load) and detwinned martensite (under load) [10].

The SMAs have a host of aspects that should be highlighted. The first one is the reversibility of the alloys, which is a measure of SME and determined by the strain persisted at the end of the complete thermal cycle. When a SMA is distorted to detwinned martensite, the total strain consists of three disparate parts: elastic strain, shape strain

(ε_{sme}), and irrecoverable strain (ε_{irr}). Shape strain refers to the strain recovered by SME in RT, and the latter defines permanent stress after the thermal cycle. The summation of elastic strain and shape strain constitutes recoverable strain (ε_{rec}). Lower ε_{irr} refers to more efficient SME and less energy dissipation through non-reversible parts.

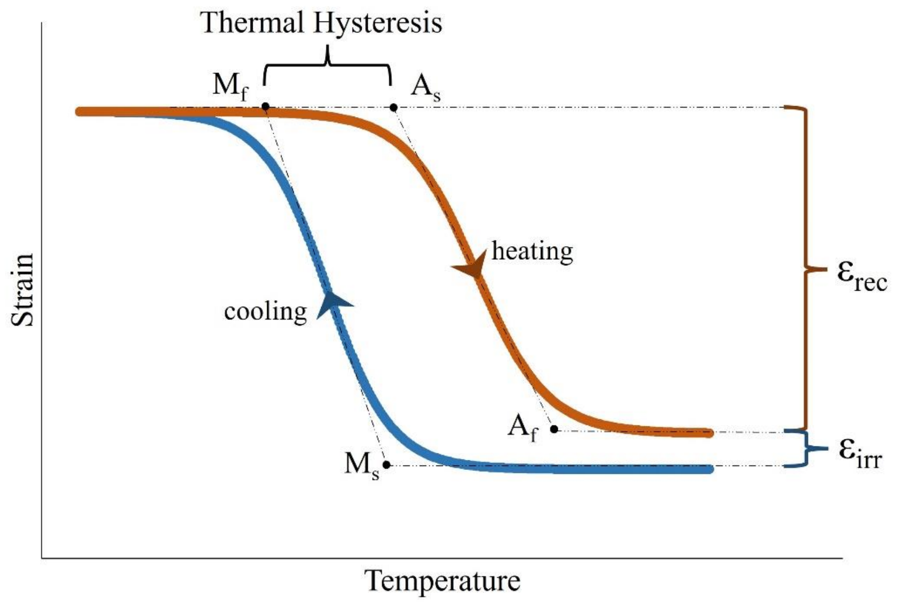

Figure 1.4. Thermal cycling under constant load [6]

The next aspect of SMAs is the thermal hysteresis, which is the difference between A_f and M_s, as shown in Figure 1.4. Thermal hysteresis displays how efficient the MT is since non-reversible mechanisms in MT result in some energy loss that raises the thermal hysteresis. SMA with a more significant thermal hysteresis requires a wide temperature range, which means more heat or energy addition for the alloy to actuate; hence, minimizing the thermal hysteresis is desired.

The cyclic stability of an SMA is also an integral aspect in terms of shape memory applications. If the transition temperatures alter each thermal cycle, phase transformations may not be complete during operation, and catastrophic failures may occur. The stability of SMAs depends strongly on microstructure. Because diffusion mechanisms are activated at elevated temperatures, a change in microstructure is more likely to happen at high operating temperatures. Thus, the cyclic stability of an SMA gains additional importance at high temperatures [6,7,9].

There are several methods to enhance the shape memory properties of the SMAs. To begin with, in order to decrease ε_{irr}, strengthening the alloy has significant importance. Enlarging the gap between martensite yield stress and the critical stress of shape memory behavior shrink plastic strain; thus, increasing the martensite yield stress by cold working at room temperature is an effective technique. Additionally, generating hard precipitates by aging treatment is another method to improve the strength of SMAs [11]. The thermally cycling of the SMAs between the parent and second phase, also known as training, can create dislocations that cause strengthening via oriented internal stress.

SMAs are incorporated in several fields, from medical to aerospace applications. Even in daily life, SMAs are utilized instead of electrical sensors due to their reliability and smaller size; for example, valves made of SMA are used for shower faucets to arrange cold and hot water flow to keep the temperature constant. The most successful and widespread utilization of SMAs can seem in a wide range of medical applications, such as orthodontic wires, nitinol drills for root canal surgery, cardiovascular stent, etc. Pseudoelasticity in the austenite phase enables the nitinol drill to rotate when it is tilted, and body temperature allows the SMA stent to enlarge in vessels. As a result, the unique properties of SMA make them special for medical applications.

Furthermore, SMAs are regarded as dampers and used for impact absorption on vehicles for military applications. There are several studies on the development of fixed-wing aircraft, rotorcraft, and spacecraft via SMAs for the aerospace industry owing to SMAs' higher power/weight ratio and simplicity than electrical counterparts. However, due to high operating temperatures, adopting SMAs for internal jet engine components or oil drilling support is an entirely disparate challenge. It requires an additional class of SMAs, namely high-temperature shape memory alloy [1,5,10,12].

The high-temperature shape memory alloys (HTSMAs) are defined as the class of SMAs which can operate temperatures beyond 100 °C. Ternary alloying of NiTi with Pt, Pd, Au, Hf, and Zr results in HTSMAs [13–15]. Mainly, HTSMAs within the 100-400 °C were studied commonly owing to variable alloy systems in this range [9]. On the other hand, as temperature increases beyond 400 °C, additional challenges emerge. Firstly, the yield stress drops with increasing temperature; hence, the difference between yield stress and the critical stress of shape memory reduces, and plastic deformation becomes more dominant. Consequently, plastic strain inclines. Besides, the strengthening mechanisms mentioned previously are not helpful for HTSMAs since dislocations created by work hardening can be relocated or recovered, and precipitates generated by aging treatment can dissolve at elevated temperatures. Change in the microstructure is another risk at high temperatures since TTs can alter based on precipitate formation, size, and volume fraction.

Among various HTSMA systems, NiTiHf alloy should be put emphasis on due to numerous advantages compared to other alloys. NiTiHf alloy possesses a reasonable temperature range compared to Ni-Ti-Zr compositions. In addition to its high operation temperature, the cost of the NiTiHf alloys is significantly lesser than the counterparts that include Pt and Pd. The increased work output and medium ductility level of NiTiHf make them valuable for high-temperature actuator production [16]. It should be noted that the properties of SMAs are sensitively dependent on their chemical compositions, which leads to extensive alloy systems to be searched, which is also valid for NiTiHf HTSMAs [17,18]. Larger search space necessitates numerous empirical studies that are expensive and time-consuming. Consequently, we searched for new alloy design methods to produce optimal NiTiHf composition.

1.2.2 Machine Learning

Machine learning (ML) is fundamentally the capability of algorithms to learn from data. First of all, the action of learning should be described in detail to understand machine learning basics. Suppose the success of a computer program in task T, measured by performance P, increases with the experience E. In that case, we can declare that the computer program is learning to accomplish task T from the supplied experience (E). Therefore, to build an acknowledged ML algorithm, the task of the model should be defined, the measure of performance should be selected, and a dataset for the model to gain experience should be prepared [19].

Learning models can be separated into particular groups according to the problem that the model tries to handle, or in other words, its task. Unsupervised learning is adopted to group the data without any particular label. Unlikely, predicting the response of data as close as possible is essential in supervised learning. Data response, which is an output column $Y = [y_1, y_2, \ldots, y_{n-1}, y_n]^T$, can be either continuous values or discrete classes. The model that deals with the former option is called regression, and the other is defined as classification. In this thesis, specifically regression models will be discussed.

Following the task's definition, the model's experience should be established, referring to an appropriate dataset. The rows of the input dataset should be constituted by various examples or instances that suit the model's task. The columns of the input set should contain examples' relevant properties, which are named feature columns. The dataset construction is significant for the success of the model, and it is detailly explained in Section 2.1. Since the input dataset is utilized for training the model, it is commonly called the *training set* and has the following form, where N is the number of features and n refers to the number of instances:

$$X = \begin{bmatrix} x_1^1 & \cdots & x_1^N \\ \vdots & \ddots & \vdots \\ x_n^1 & \cdots & x_n^N \end{bmatrix} \tag{1.1}$$

Designing a measure of performance or loss is another challenge to be overcome. First of all, the final performance should be determined on new data that the model has not seen before because it allows estimating the model's success in the real world. Thus, separating a *test dataset* for the final performance evaluation is essential. Additionally, a quantitative function should be defined to evaluate the model's performance, called the cost function. The decision of the cost function should be made based on the corresponding desired behavior of the system. To exemplify, one can prefer frequently distributed medium-sized errors to rare but huge mistakes. Penalizing the huge errors is more accurate for this circumstance. The coefficient of determination (R^2) parameter, which describes the goodness of the fit, and the mean squared error (MSE), the measure of the expected value of Euclidean distance between actual and predicted output, are two commonly used cost functions in ML applications. Their formulations are supplied in equations (1.2) and (1.3), respectively, where $\hat{y}$ represents the predicted value, and $\bar{y}$ stands for mean value of the output column Y [20,21].

$$R^2 = 1 - \frac{\sum_{i=1}^{n}(\hat{y_i} - y_i)^2}{\sum_{i=1}^{n}(\bar{y_i} - y_i)^2} \tag{1.2}$$

$$MSE = \frac{1}{n}\sum_{i=1}^{n}(\hat{y_i} - y_i)^2 \tag{1.3}$$

To sum up, the learning process can be described with the following steps. Initially, a comprehensive dataset that includes relevant features is constructed by search and data collection. It is followed by appropriate model selection in accordance with the task aimed. Then, the dataset is separated into training and test data. While the former is trained by the model to build a formulation that describes the relationship between input and output, the latter is kept for determining the score of the model at the end. Training is an iterative process in which the model slightly changes weights assigned to minimize its training cost via a selected optimizer. When the cost is minimized, the model is utilized to predict the outputs of the test dataset, and the performance of the model is calculated with test predictions and actual values. Here, it should be highlighted that the model's performance is evaluated with the test dataset despite the training cost calculated by the training dataset. This method is preferred to retain the generalization of the model, which refers that the model can explain all data reasonably instead of explaining some data perfectly but neglecting the rest. To comprehend the generality of the model, two terms should be described: underfitting and overfitting [19,22].

Underfitting regards the condition when the model is too simple to fulfill the task. It can be detected from high training and test errors and quickly overcome by utilizing more complex models. On the contrary, overfitting occurs if the model is too complicated to explain training data excellently but fails for the test dataset. In other words, the model suffers from underfitting if it is too general, and it suffers from overfitting if it is too specific. Therefore, building a sufficiently generalized model is the fundamental condition for a successful model. To ensure the generalization of the model, regularization, which prevents less critical features from dominating the model, is one of the well-known methods embedded into the algorithm. Regularization inserts an additional penalty term, a function of weights, to the cost function to avoid enormous weights. Two successful regularization methodologies are commonly adopted: Lasso (L1) and Ridge (L2) regularizations. Penalty terms used for updating the cost function are supplied in equations (1.4) and (1.5), respectively, where α refers to regularization parameter, and w represents weight of feature i.

$$Cost\ Function = Training\ Performance + \alpha \sum_{i=0}^{N} |w_i| \tag{1.4}$$

$$Cost\ Function = Training\ Performance + \alpha \sum_{i=0}^{N} w_i^2 \tag{1.5}$$

If the regularization parameter equals zero, the equation becomes simple cost function without any regularization. On the contrary, as α increases summation of weights term should decline to minimize cost function; consequently, unnecessarily higher weights which may lead to overfitting are removed. One critical difference between Lasso and Ridge regression is that while the former can converge weights to 0, the latter cannot. Therefore, Lasso regression can be employed as a feature selection algorithm. On the other hand, Ridge regression can handle correlated features better than Lasso regression [23].

The artificial neural network (ANN), developed significantly for the last few decades, is a distinguishable computational methodology among numerous ML models. The neural networks (NNs) combine layers of computing nodes with building complex connections between weights similar to their original inspiration from biological neurons. The first NN was introduced by Rosenblatt in 1959 [24] as a simple linear algorithm; however, fifteen years later, Werbos developed a nonlinear NN model [25]. With the addition of hidden layers, the actual capability of NN to estimate arbitrary nonlinear functions was recognized.

An ANN structure consists of an input layer, an output layer, and an adjustable number of hidden layers, as illustrated in Figure 1.5. Despite the dimensions of input and output layers being restricted by the shape of the dataset, the number of nodes in the hidden layers can vary. The input matrix is multiplied with a weight tensor, then transferred to the first hidden layer. By transforming the data into a new space with an activation function, the NN model can powerfully turn linear formulations into nonlinear expressions and convey them to the next hidden layer. Similar to the other ML models, weights are iteratively adjusted with an optimizer function according to the selected cost function.

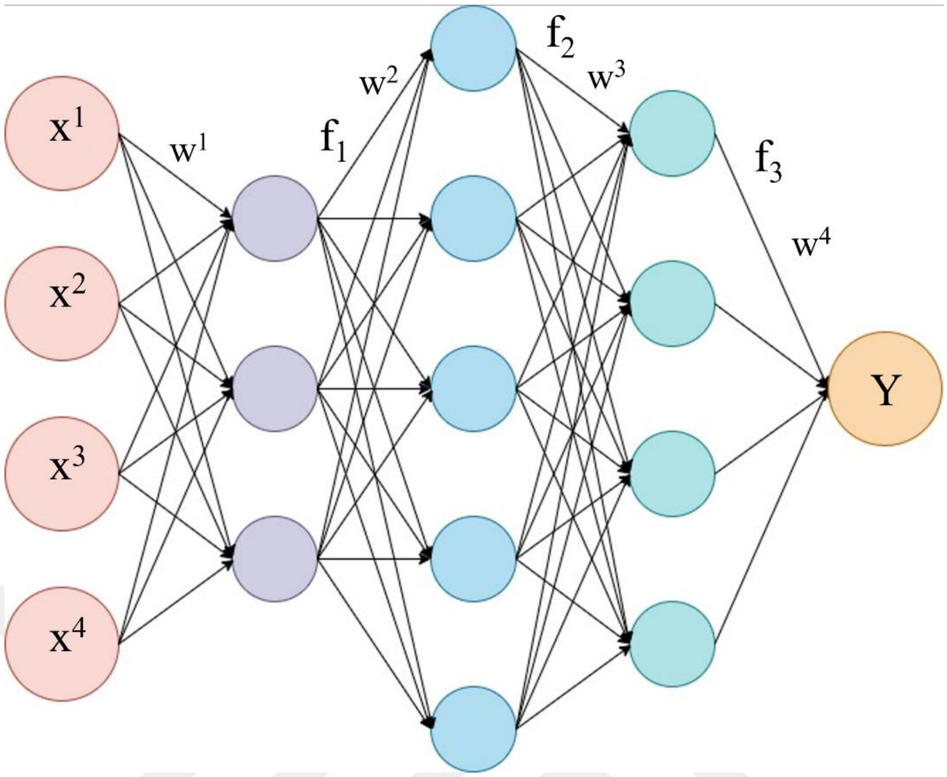

Figure 1.5. A multilayer feedforward neural network structure with three hidden layers where layers contain 3, 5, and 4 nodes, respectively

The ANN structure illustrated in Figure 1.5 can be mathematically formulated by the following expression:

$$f_3\left(f_2\left(f_1\left(\begin{bmatrix} x_1^1 & \cdots & x_1^4 \\ \vdots & \ddots & \vdots \\ x_n^1 & \cdots & x_n^4 \end{bmatrix}_{n\times 4} \times \begin{bmatrix} w_1^{1,1} & \cdots & w_1^{1,3} \\ \vdots & \ddots & \vdots \\ w_4^{1,1} & \cdots & w_4^{1,3} \end{bmatrix}_{4\times 3}\right) \times \begin{bmatrix} w_1^{2,1} & \cdots & w_1^{2,5} \\ \vdots & \ddots & \vdots \\ w_3^{2,1} & \cdots & w_3^{2,5} \end{bmatrix}_{3\times 5}\right) \times \begin{bmatrix} w_1^{3,1} & \cdots & w_1^{3,4} \\ \vdots & \ddots & \vdots \\ w_5^{3,1} & \cdots & w_5^{3,4} \end{bmatrix}_{5\times 4}\right) \times \begin{bmatrix} w_1^{4,1} \\ \vdots \\ w_4^{4,1} \end{bmatrix} = \begin{bmatrix} y_1 \\ \vdots \\ y_n \end{bmatrix} \tag{1.6}$$

where, f represents the activation function, and w refers to components of weight tensor W. The dimensions of weight tensors vary from model to model depending on the desired complexity of the model. For prohibiting underfitting and overfitting, the optimal dimension of tensors should be determined by trial-and-error methodologies [26].

The capability of ANN to solve nonlinear problems is based on the activation function that projects internal outputs of the nodes in the hidden layer (Z) into a nonlinear space. There are multiple options as activation functions popular in literature. Hyperbolic tangent, formulated by $f(Z) = \frac{e^Z - e^{-Z}}{e^Z + e^{-Z}}$, and sigmoid function, which is expressed by $f(Z) = \frac{1}{1+e^{-Z}}$ are the earlier commonly adopted activation functions. Recently, rectified linear unit (ReLU), $f(Z) = \max(0, Z)$ substitute them due to its computational efficiency [19]. As demonstrated in Figure 1.6, ReLU has two possible derivatives that enable it to be computed faster in gradient calculations.

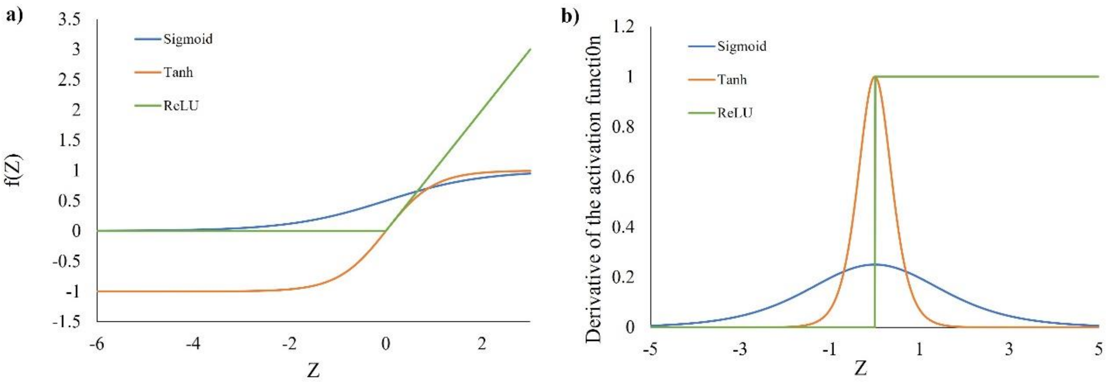

Figure 1.6. Various activation functions utilized in NN models

1.3 Objective

Plentiful search space in material science and the expensive investment for the design of experiments motivated researchers to develop an alternative methodology. The ML implementation in material science, therefore, drew noticeable interest due to its capability in prediction with unexplored inputs. The application of ML facilitates not only saving of time and source but also comprehensive research on the selected field due to the necessity of data collection.

Recent studies on ML implementation in material science have proven its capability in alloy design [27–35]. We particularly paid attention to works on NiTi-based SMAs in which the TTs were predicted via integrating ML models with material information, such as chemical and electronic structures. The prospering outcomes of the studies are the evidence of a new successful design methodology without the extended time and source consumption.

In the light of the given background, the demand for affordable NiTiHf with elevated operation temperatures in the aerospace and oil industry and the aforementioned examples of successfully applied ML algorithms on material science encouraged us to combine these two fields. In the current work, the main objective is designing a thermally stable NiTiHf composition with A_f temperature beyond 400 °C and relatively low thermal hysteresis with the assist of ML algorithms.

1.4 *References*

[1] A. Nespoli, S. Besseghini, S. Pittaccio, E. Villa, S. Viscuso, The high potential of shape memory alloys in developing miniature mechanical devices: A review on shape memory alloy mini-actuators, Sensors Actuators, A Phys. 158 (2010) 149–160. https://doi.org/10.1016/j.sna.2009.12.020.

[2] G. Kurdyumov, L. Khandros, On the “Thermoelastic” Equilibrium on Martensitic Transformations (Reprint 2008), Dokl. Akad. Nauk SSSR. 66 (1949) 211–214.

[3] W.J. Buehler, J. V. Gilfrich, R.C. Wiley, Effect of Low-Temperature Phase Changes on the Mechanical Properties of Alloys near Composition TiNi, J. Appl. Phys. 34 (1963) 1475–1477. https://doi.org/10.1063/1.1729603.

[4] H.C. Donkersloot, J.H.N. Van Vucht, Martensitic Transformations in Gold-Titanium, Palladium-Titanium and Platinum-Titanium Alloys Near The Equiatomic Composition, J. Less-Common Met. 20 (1970) 83–91.

[5] D.J. Hartl, D.C. Lagoudas, Aerospace applications of shape memory alloys, Proc. Inst. Mech. Eng. Part G J. Aerosp. Eng. 221 (2007) 535–552. https://doi.org/10.1243/09544100JAERO211.

[6] K. Otsuka, C.M. Wayman, Shape Memory Materials, Cambridge University Press, Cambridge, 1999. https://books.google.com.tr/books?id=DvItE9XUlN8C.

[7] C. Lexcellent, Shape-memory Alloys Handbook, John Wiley & Sons, Inc., Hoboken, NJ, USA, 2013. https://doi.org/10.1002/9781118577776.

[8] M. Fremond, S. Miyazaki, Development and Characterization of Shape Memory Alloys. In: FREMOND, M.; MIYAZAKI, S. Shape Memory Alloys., Springer-Verlag Wien, 1996. https://doi.org/10.1007/978-3-7091-4348-3 ISBN.

[9] J. Ma, I. Karaman, R.D. Noebe, High temperature shape memory alloys, Int. Mater. Rev. 55 (2010) 257–315. https://doi.org/10.1179/095066010X12646898728363.

[10] D.C. Lagoudas, Shape Memory Alloys: Engineering Application, 2016.

[11] H.E. Karaca, S.M. Saghaian, G. Ded, H. Tobe, B. Basaran, H.J. Maier, R.D. Noebe, Y.I. Chumlyakov, Effects of nanoprecipitation on the shape memory and material properties of an Ni-rich NiTiHf high temperature shape memory alloy, Acta Mater. 61 (2013) 7422–7431. https://doi.org/10.1016/j.actamat.2013.08.048.

[12] J. Van Humbeeck, Non-medical applications of shape memory alloys, Mater. Sci. Eng. A. 273–275 (1999) 134–148.

[13] J.A. Monroe, I. Karaman, D.C. Lagoudas, G. Bigelow, R.D. Noebe, S. Padula, Determining recoverable and irrecoverable contributions to accumulated strain in a NiTiPd high-temperature shape memory alloy during thermomechanical cycling, Scr. Mater. 65 (2011) 123–126. https://doi.org/10.1016/j.scriptamat.2011.03.019.

[14] D. Canadinc, W. Trehern, J. Ma, I. Karaman, F. Sun, Z. Chaudhry, Ultra-high temperature multi-component shape memory alloys, Scr. Mater. 158 (2019) 83–87. https://doi.org/10.1016/j.scriptamat.2018.08.019.

[15] P.K. Kumar, D.C. Lagoudas, Experimental and microstructural characterization of simultaneous creep, plasticity and phase transformation in Ti50Pd40Ni10Ti50Pd40Ni10 high-temperature shape memory alloy, Acta Mater. 58 (2010) 1618–1628. https://doi.org/10.1016/j.actamat.2009.11.006.

[16] H.E. Karaca, E. Acar, H. Tobe, S.M. Saghaian, NiTiHf-based shape memory alloys, Mater. Sci. Technol. (United Kingdom). 30 (2014) 1530–1544. https://doi.org/10.1179/1743284714Y.0000000598.

[17] T. Umale, D. Salas, B. Tomes, R. Arroyave, I. Karaman, The effects of wide range of compositional changes on the martensitic transformation characteristics of NiTiHf shape memory alloys, Scr. Mater. 161 (2019) 78–83. https://doi.org/10.1016/j.scriptamat.2018.10.008.

[18] D.R. Angst, P.E. Thoma, M.Y. Kao, The Effect of Hafnium Content on the Transformation Temperatures of Ni 49 Ti 51-x Hf x . Shape Memory Alloys , J. Phys. IV. 05 (1995) C8-747-C8-752. https://doi.org/10.1051/jp4/199558747.

[19] Yoshua Bengio, I.J.G.A. Courville, Deep Learning, Eur. Univ. Inst. (2015).

[20] J. Bossart, Opening the black box, Pharm. Manuf. Pack. Sourcer. (2010) 32–34. https://doi.org/10.5860/crl.77.5.564.

[21] T.O. Kvålseth, Cautionary Note about R 2, Am. Stat. 39 (1985) 279–285. https://doi.org/10.1080/00031305.1985.10479448.

[22] M. Kuhn, K. Johnson, Applied Predictive Modeling, Springer New York, New York, NY, 2013. https://doi.org/10.1007/978-1-4614-6849-3.

[23] H. Zou, T. Hastie, Regularization and variable selection via the elastic net, J. R. Stat. Soc. Ser. B Stat. Methodol. 67 (2005) 301–320.

https://doi.org/10.1111/j.1467-9868.2005.00503.x.

[24] B.W. White, F. Rosenblatt, Principles of Neurodynamics: Perceptrons and the Theory of Brain Mechanisms, Am. J. Psychol. 76 (1963) 705. https://doi.org/10.2307/1419730.

[25] P.J. Werbos, Beyond regression: New tools for prediction and analysis in the behavioral sciences., 1975.

[26] G. John, R. Kohavi, K. Pfleger, Irrelevant Features and the Subset Selection Problem, in: Mach. Learn. Proc. Elev. Int. Conf., 1994: pp. 121–129. http://machine-learning.martinsewell.com/feature-selection/JohnKohaviPfleger1994.pdf.

[27] A. Nazarahari, D. Canadinc, Prediction of the NiTi shape memory alloy composition with the best corrosion resistance for dental applications utilizing artificial intelligence, Mater. Chem. Phys. 258 (2021) 123974. https://doi.org/10.1016/j.matchemphys.2020.123974.

[28] W. Huang, P. Martin, H.L. Zhuang, Machine-learning phase prediction of high-entropy alloys, Acta Mater. 169 (2019) 225–236. https://doi.org/10.1016/j.actamat.2019.03.012.

[29] D. Xue, D. Xue, R. Yuan, Y. Zhou, P. V. Balachandran, X. Ding, J. Sun, T. Lookman, An informatics approach to transformation temperatures of NiTi-based shape memory alloys, Acta Mater. 125 (2017) 532–541. https://doi.org/10.1016/j.actamat.2016.12.009.

[30] S. Liu, B.B. Kappes, B. Amin-ahmadi, O. Benafan, A.P. Stebner, X. Zhang, A physics-informed feature engineering approach to use machine learning with limited amounts of data for alloy design: shape memory alloy demonstration, (2020) 1–32. http://arxiv.org/abs/2003.01878.

[31] D. Xue, Y. Tian, R. Yuan, T. Lookman, Bayesian Global Optimization applied to the design of shape-memory alloys, Elsevier Ltd, 2020. https://doi.org/10.1016/b978-0-08-102941-1.00016-x.

[32] C. Wen, Y. Zhang, C. Wang, D. Xue, Y. Bai, S. Antonov, L. Dai, T. Lookman, Y. Su, Machine learning assisted design of high entropy alloys with desired property, Acta Mater. 170 (2019) 109–117. https://doi.org/10.1016/j.actamat.2019.03.010.

[33] Q. Wu, Z. Wang, X. Hu, T. Zheng, Z. Yang, F. He, J. Li, J. Wang, Uncovering

the eutectics design by machine learning in the Al–Co–Cr–Fe–Ni high entropy system, Acta Mater. 182 (2020) 278–286. https://doi.org/10.1016/j.actamat.2019.10.043.

[34] X. Hu, J. Wang, Y. Wang, J. Li, Z. Wang, Y. Dang, Y. Gu, Two-way design of alloys for advanced ultra supercritical plants based on machine learning, Comput. Mater. Sci. 155 (2018) 331–339. https://doi.org/10.1016/j.commatsci.2018.09.003.

[35] N. Islam, W. Huang, H.L. Zhuang, Machine learning for phase selection in multi-principal element alloys, Comput. Mater. Sci. 150 (2018) 230–235. https://doi.org/10.1016/j.commatsci.2018.04.003.

Chapter 2:
MODEL

2.1 *Dataset Preparation*

Regardless of the model's capability in predicting, the dataset preparation is an integral part of machine learning because each information interpreted by the model is supplied by an appropriate dataset. Determination of related properties to be gathered and distinction of related and redundant features, therefore, play a critical role in a successful ML implementation. Consequently, in this work, the aspects that have an impact on shape memory properties were searched in detail before collecting data which were mentioned in detail in the previous section. The chemical composition, grain size, precipitate size and volume fraction, and thermo-mechanical heat treatments were specified as major parameters in shape memory alloys. However, microstructural properties, i.e., features related to grains and precipitates, could not contribute to the dataset due to devoid of required information in previous works. As a result, chemical composition and applied thermo-mechanical heat treatments were accumulated in the dataset utilized in the current work.

Another crucial point in dataset preparation is deciding the range of the training dataset. Even though the training set should be as large as possible to reflect a general relation between given inputs and output, some constraints are required to avoid abundant data, which may have the model deviate from its aim. Because the main objective of this work is to predict a composition with high TTs, gathering the data of the same composition under different experimental conditions is redundant. To illustrate, two samples with identical chemical composition and microstructure can have different A_f temperature if it is measured in thermal cycles under distinct loads; however, this phenomenon can be explained by the Clasius-Clayperon relation. Thus, collecting both of these data creates additional work for the model, and the algorithm may focus on solving stress-TTs relation instead of the primary goal. The dataset, therefore, was restricted to the experiments under zero load, in other words, DSC experiments. Moreover, we gathered data from the first thermal cycle since the stability search was out of the scope of this work.

An elaborative literature review has been done under the aforementioned constraints to prepare an appropriate dataset of NiTiHf alloys. However, gathering information from others' work creates several issues such as reliability and unnoticeable experimental error. Fortunately, avoiding these problems is possible by the elimination of data. To clarify, although different researchers conduct identical experiments on the same composition, their results may not overlap due to any possible mistake during the experiment. Consequently, multiple disparate outcomes, referred to as conflicted instances hereafter, emerge. The conflicted instances have to be omitted; otherwise, an increase in error is inevitable since a successful prediction of one of them causes the other to be predicted unsuccessfully. As a result, solely one example in a group of conflicted instances was kept in the dataset, and the rest was eliminated. Closeness to the mean value of a certain conflicted instance group is the primary criterion for selecting the instance retained. The elimination of conflicted instances resulted in a dataset consisting of 255 instances that belong to 66 different compositions [1-44]. The distribution of data with respect to atomic % of Hf content is supplied in Figure 2.1.

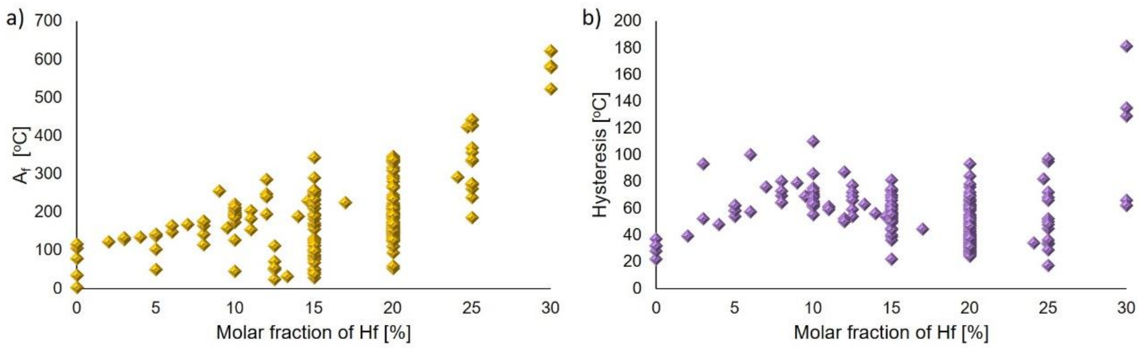

Figure 2.1. Distribution of dataset according to the corresponding at.% of Hf content [45]

Gaussian distribution of dataset plays a critical role in regression models. However, the thermo-mechanical treatment information gathered accumulates around some specific treatment methods commonly used by researchers, which prohibit Gaussian distribution. Furthermore, several NiTiHf compositions, such as $Ni_{50.3}Ti_{29.7}Hf_{20}$, are popular among researchers, leading them to outnumber other compositions in the dataset. This fact may cause the ANN algorithm to focus on thermo-mechanical treatment features instead of the alloy composition, which is the central goal of this work. Consequently, to protect both Gaussian distribution and the importance of molar fractions, we prepared a second dataset containing only different compositions.

In the preparation of the second dataset, selecting compositions with similar treatment was essential to decrease the effectiveness of various thermo-mechanical treatments on the microstructure of the alloys. Therefore, checking the thermo-mechanical treatment similarity was our primary concern. Some compositions, however, did not have an example with a similar treatment to the second dataset. Nevertheless, every different composition was valuable due to a lack of data. Consequently, for compositions with disparate treatments, the datum with an output closest to the mean of that compositions' output was selected for the second dataset. A second dataset with 66 instances was created by paying attention to these criteria. This new dataset was especially beneficial to predict A_f since TTs are remarkably sensitive to microstructural change and may vary with various thermo-mechanical treatments.

Normalization of the dataset is another fundamental step in data preparation. For a dataset consisting of features with a distinct range, like ours, the feature columns involving higher numbers can simply dominate the algorithm and cause overfitting. To obstruct this, the model has to decrease the weight of the dominant feature and increase the weight of the features consisting of lower numbers. This circumstance requires a vast gap between weights which is hard to obtain for similarly initialized weights; therefore, it may prevent convergence of the algorithm. However, normalization can easily overcome this problem by normalizing data between 0 and 1 without changing the distribution. As a result, all feature columns were normalized to this range by the formula below (*2.1*), where x_i represent the ith instance in feature column *x*, and x_i' refers to its normalized version. $(x)_{\max}$ and $(x)_{min}$ are the maximum and the minimum values of feature *x*.

$$x_i' = \frac{x_i - (x)_{min}}{(x)_{\max} - (x)_{min}} \tag{2.1}$$

A well-known and straightforward transformation technique, which is taking square root, was adopted to obtain more Gaussian distribution. As a measure of how symmetrically the dataset distributed, the skewness parameter was evaluated by equation (2.2), where *n* is the number of instances, y_i is ith instance and $\bar{y}$ represents the average of the corresponding output column.

$$skewness = \frac{\sum (y_i - \bar{y})^3}{(n-1)\sqrt{\left(\frac{\sum (y_i - \bar{y})^2}{n-1}\right)^3}}$$

(2.2)

The skewness parameter indicates the symmetry of the dataset [46]. When it gets closer to zero, the probabilities of the datum to be bigger or smaller than the mean value approaches. As a result, the data distribute more Gaussian. Figure 2.2 illustrates the histogram of A_f and thermal hysteresis outputs with calculated skewness parameters. By taking the square root of the data, both skewness parameters shrank, which overlaps the histograms where the data distribution alters more Gaussian versions.

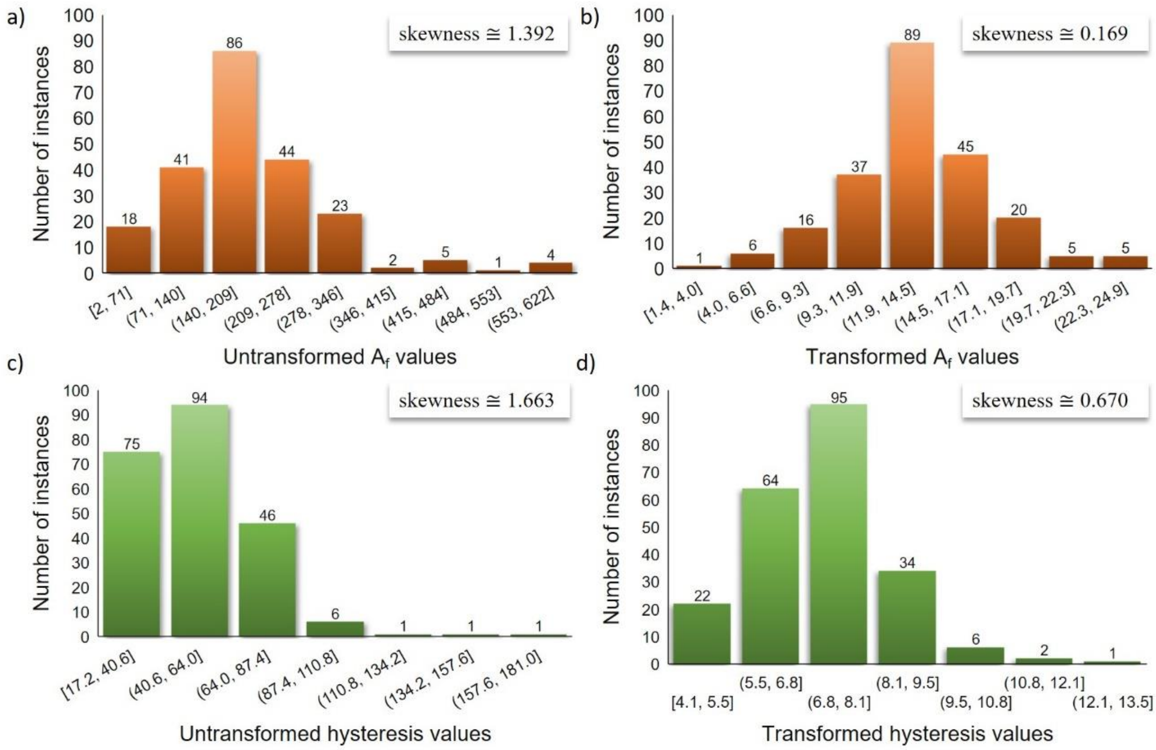

Figure 2.2. Distributions of (a) untransformed A_f, (b) transformed A_f, (c) untransformed thermal hysteresis, and (d) transformed thermal hysteresis data.[45]

2.2 Model details

An MLFFNN model with five hidden layers was adopted as an ML algorithm due to its aforementioned success in prediction. The MSE was selected for the cost function of the model, which is optimized by an adaptive moment estimation (adam) optimizer in each iteration. The activation function between hidden layers was chosen as rectified linear unit (RELU) function. Ridge regression, also known as L2 regression, was employed to avoid overfitting. The capability of Ridge regression to handle highly correlated features causes it to be preferred instead of Lasso regression. The dataset was randomly shuffled to ensure homogeneity; hence, the bias while splitting data into training and test sets was avoided. The ANN model was established with the TensorFlow framework, and well-known libraries, namely SciPy, sci-kit learn, and matplotlib via Python [47-50]. In Figure 2.3, the model utilized in the current work is illustrated. The activation function that transforms the last hidden layer to output was chosen as a linear function to protect continuity.

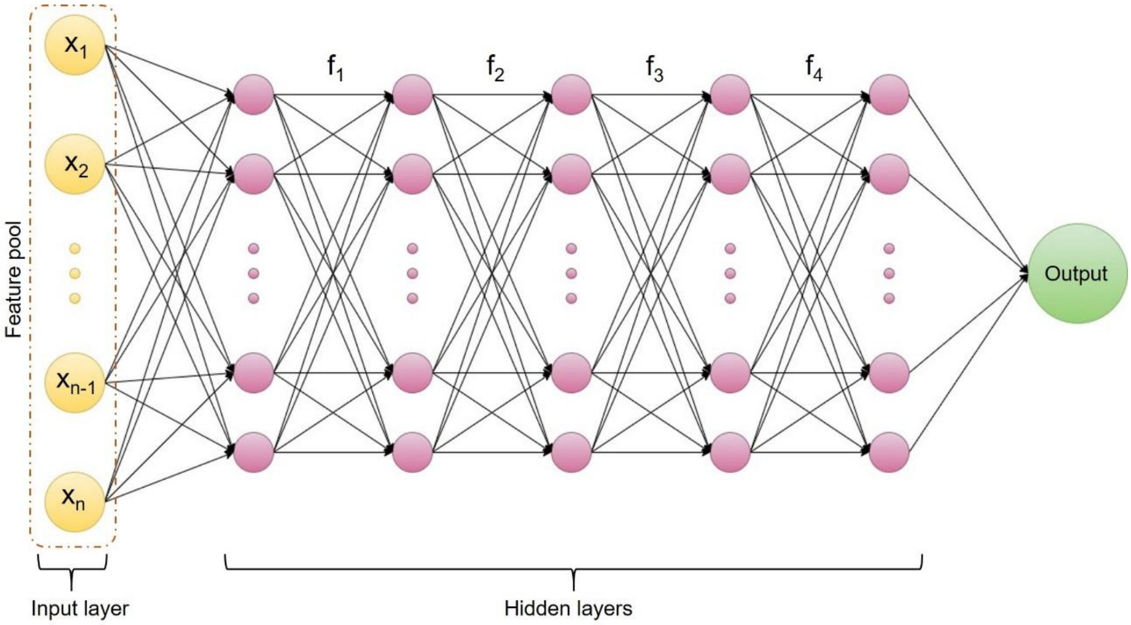

Figure 2.3. An illustration of the ANN model utilized [45]

2.3 Feature selection

One of the integral steps for a successful prediction is specifying features that include relevant information to the target. Hence, the SME and several material aspects that may impact shape memory properties have been examined in detail in the current study.

The first property, namely the average valence electron number of the alloy, was considered due to its discovered relation to TTs. Zarinejad et al. mainly focused on the electronic structure of the NiTi-based SMAs to figure out the control mechanism of these alloys [38]. In their work, 50 different solution-treated NiTi-based SMAs have been investigated in terms of atomic bonding. They selected the valence electron number as the measure of the atomic bond based on the fact that the valence electrons compose metallic bonds by holding the rest of the electrons and ion core together. As a result, the valence electron number per atom and the valence electron concentration (c_v) were determined as the parameters in their work. These terms can be calculated by the following equations (equations (*2.3* and (*2.4*).

$$\frac{e_v^{alloy}}{atom} = f_{Ni}e_v^{Ni} + f_{Ti}e_v^{Ti} + e_v^{Hf} \tag{2.3}$$

$$c_v = \frac{e_v^{alloy}}{f_{Ni}Z_{Ni} + f_{Ti}Z_{Ti} + f_{Hf}Z_{Hf}} \tag{2.4}$$

where, e_v^i, f_i and Z_i are the valence electron number, atomic fraction, and atomic number of the element i, respectively, while $\frac{e_v^{alloy}}{atom}$ represents valence electron number per atom. Their works demonstrated a trend between valence electron number per atom and TTs. TTs decrease with the increasing valence electron per atom except for the region between the valence electron per atom of 6.8 and 7.2. Zarinejad et al. attributed this interesting observation mainly to the complete d-d overlapping electron occupancy. The c_v, on the other hand, showed a similar trend without any exception. According to their study, the relation between TTs and c_v can be explained by the number of valence electrons in the unit volume of the cell; in other words, valence electron density (VED). While the c_v and VED are proportional due to their similar denominators, the mechanism behind the relation between VED and TTs is more convoluted. The contribution of Gilman et al. displays dependence of bulk modulus on the VED: an increase in the VED causes the former to increase [51]. The shear modulus, which is generally equal to 3/5 of bulk modulus for metals, therefore, rises with the increasing VED. A metal with a higher shear modulus has a higher resistance to shape change, which obstructs martensitic phase transformations and requires more energy or enormous temperature difference. To illustrate, if the modulus of austenite is higher, it necessitates lower M_s to meet energy needs. Unfortunately, the alloys' unit cell volume is generally unavailable in the literature; hence, VED could not be adopted as a feature. Moreover, adding the valence electron per atom to the dataset was redundant since solely Ni has a different valence electron number, resulting in a complete correlation between the atomic fraction of the Ni and the valence electron number per atom. Consequently, the only c_v which displayed the desired relation, as shown in Figure 2.4, has been kept in the feature set.

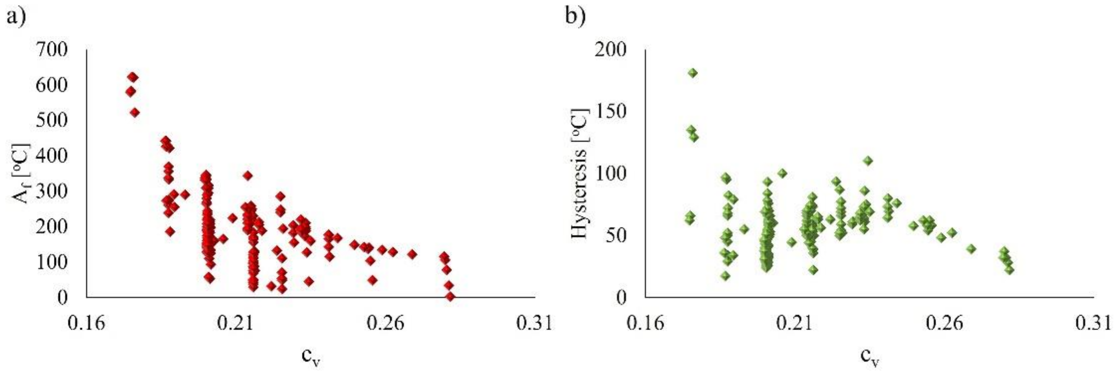

*Figure 2.4. Distribution of A_f **(a)** and thermal hysteresis **(b)** according to valence electron concentration [45]*

The dimension of components is the next property that has a remarkable impact on shape memory properties. The atomic radius, ionic radius, and Waber-Cromer's pseudopotential radius have been considered as a measure of size. The importance of the elements' dimension can be analyzed by comparing two disparate phases. The compatibility between austenite and martensite phases is crucial for dissipated energy that creates the defects. If the phases are more compatible, it is more likely to observe single variant martensite which does not have the boundaries, in other words, main crack initiation zones. Therefore, the compatibility between phases is desired, which is theoretically defined by the condition of λ_2=1, where λ_2 is the middle eigenvalue of the martensite to austenite transformation stretch tensor [52]. For martensite (B19') to austenite (B2) transformation, λ_2 equals $b/(a_0\sqrt{3})$ where b and a_0 are lattice parameters of martensite and austenite phases, respectively [40]. Since the dimension of the elements determines the lattice parameters in the phases, compatibility between phases is directly related to the radius of elements. As a result, the atomic radius, ionic radius, and Waber-Cromer's pseudopotential radius were adopted as features since information about lattice parameters was not generally available in the literature.

Another selected feature is the electronegativity of the elements. Electronegativity is the measure of how much an atom is willing to take an additional electron; hence, an atom with higher electronegativity attracts the electrons of an atom with lower electronegativity. If the difference between the electronegativities of species raises, they tend to form a compound instead of an alloy. On the other hand, if the electronegativity difference is too low, the metallic bond would be weak, and the entropy dominates the system. Therefore, one can conclude based on Hume-Rothery rules that the electronegativities of two alloys should be comparable to form a strong metallic bond by substituting Ti atoms with Hf.

Finally, the alloy's melting temperature is significant since it gives information about the temperature range to apply aging treatments and solution heat treatment. Suppose an alloy's melting temperature is close to the targeted operation temperature, the risk of a change in microstructure increases. Consequently, the thermal stability of the alloy is related to its melting temperature. Because the melting point data are unavailable in literature for most of the NiTiHf SMAs, we assumed that the contribution of each element's melting point could be added separately.

The average values of selected features for the corresponding composition were calculated by the following formula (equation (*2.5*), where x_i is the feature x of the element i.

$$x_{alloy} = f_{Ni}x_{Ni} + f_{Ti}x_{Ti} + x_{Hf} \tag{2.5}$$

With the addition of new features, the dimension of the feature set increased to 16, which is constituted by molar fractions of Ni *(ni)*, Ti *(ti)*, and Hf *(hf)*, the valence electron concentration *(c_v)*, average electronegativity *(pen)*, atomic radius *(ar)*, ionic radius *(ir)*, Waber-Cromer's pseudopotential radius *(wcr)*, atomic mass *(am)*, melting temperature *(mt)*, homogenization temperature *(homT)* and time *(homt)*, solution heat treatment temperature *(shtT)* and time *(shtt)*, and aging temperature *(agT)* and time *(agt)*. Properties of the elements are supplied in Table 0.1 in Appendix. Additional features were also normalized by equation (2.1).

It should be noted that adding new relevant features does not necessitate enhanced model performance. Especially, the addition of highly correlated features can create unnecessary complexity for the model and increase the computational time. Thus, the correlation between features should have been checked by the Pearson correlation, whose formula is supplied in equation (2.6)[53].

$$\rho_{i,j} = \frac{cov(x_i, x_j)}{\sigma_i \sigma_j}$$

(2.6)

where $\rho_{i,j}$ is the Pearson correlation between features x_i and x_j, σ_i is the standard deviation of the feature x_i, and $cov(x_i, x_j)$ represents the covariance between features x_i and x_j. The formulation of covariance and the standard deviation is supplied in equations (2.7) and (2.8), where $E[x]$ refers to the mean value of feature x.

$$cov(x_i, x_j) = E[x_i^T x_j] - E[x_i]E[x_j]$$

(2.7)

$$\sigma_i = \sqrt{E[x_i^T x_i] - (E[x_i])^2}$$

(2.8)

The Pearson correlation coefficient can take a value between -1 and 1, where the former stands for a complete negative correlation, and the latter refers to a total positive correlation between variables. It should be emphasized that, for standardized features, i.e., the mean of the features equals zero, the correlation coefficient is identical to the slope of the regression line between features [53]. Therefore, a complete correlation indicates that the variables are actually the same, which is abundant. The coefficient equal to 0, on the other hand, shows that the features are unrelated and may uncover different parts of the problem.

In our dataset, highly correlated variables were considerably possible since the additional features were evaluated by manipulating atomic fractions with chemical properties. Thus, the Pearson correlation map was generated, as illustrated in Figure 2.5. The size of the bubbles indicates the absolute value of the correlation between corresponding variables in Figure 2.5. The two variables, which have the highest total correlation, namely the atomic fraction of Hf and average melting temperature, are covered with dash lines. As shown in Figure 2.6, these two variables contain the same information, which is redundant to increase the model's score.

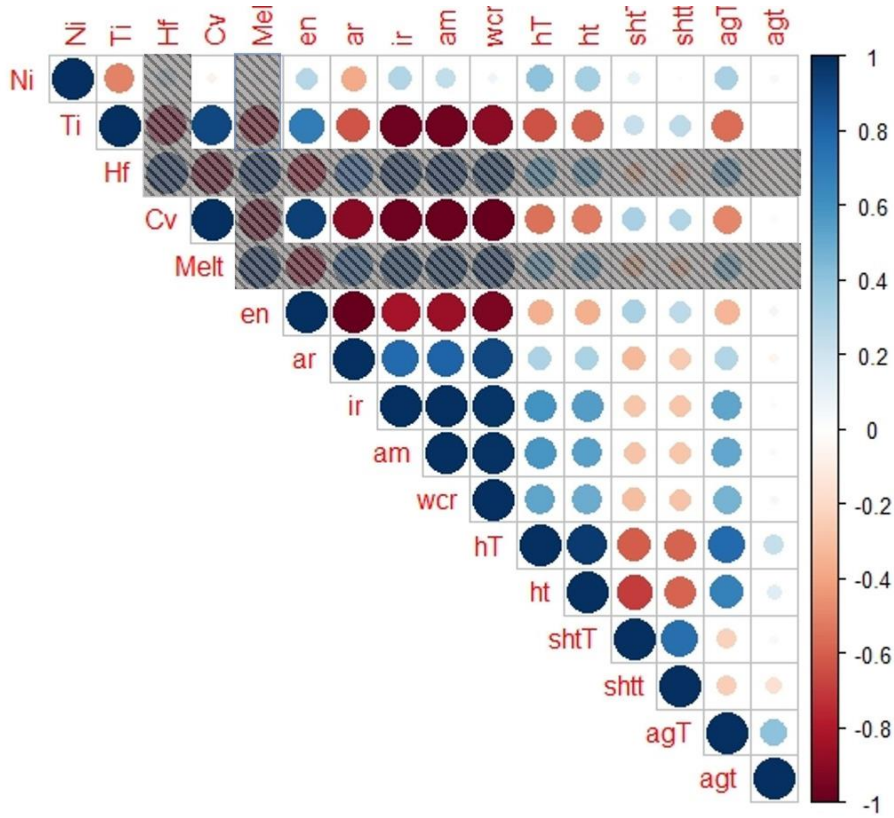

Figure 2.5. The Pearson correlation map of the feature set [45]

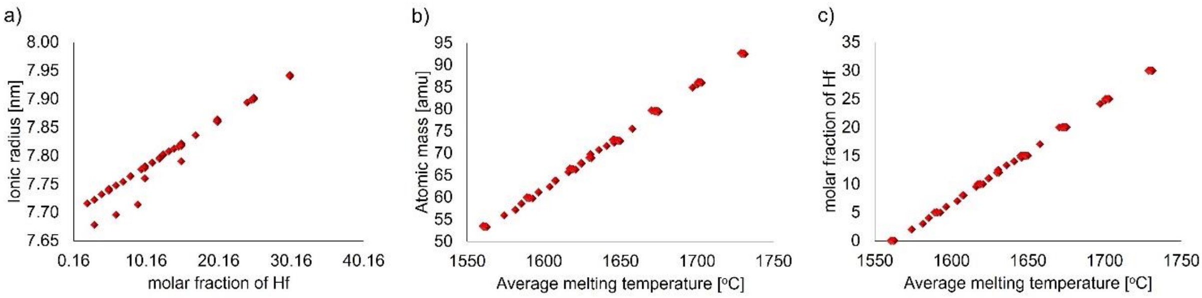

Figure 2.6. The features with high correlation

To detect the feature importance in an ANN model is not that simple compared to more basic models such as linear regression. The ANN acts as a black box, in which the interaction of the features is not as predictable as in linear models. To exemplify, two unimportant features can compose important information for the model. Consequently, instead of determining the feature importance separately, we focused on the efficiency of several feature subsets. Among various feature selection methodology, therefore, the *wrapper method* and embedded methods were utilized. The selected embedded method in the model is Ridge regression, as mentioned previous section.

The wrapper method, proposed by G. H. John and R. Kohavi [54], drew attention recently. Unlike simple filter methodologies, which can assess feature importance before training, the wrapper approach uses the model itself to determine the optimal feature subset, regardless of the type of the ML model. The wrapper method considers the model a black box, which is perfectly suitable for the ANN, and interprets the feature subsets by their impact on the prediction performance. In Figure 2.7, a chart is given to summarize the wrapper approach.

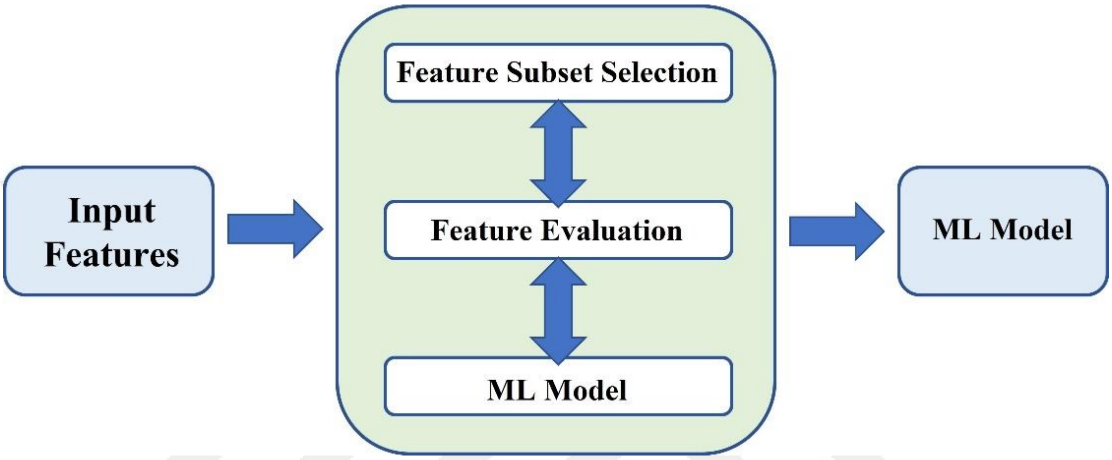

Figure 2.7. The progress chart of the wrapper approach [54]

As shown in Figure 2.7, the wrapper method requires evaluating the model for each subset; hence, its major drawback is the necessary massive computational effort. Since our input features consist of 16 variables, a host of feature combinations emerges. However, examining each subset demands enormous computational time, which is not the most efficient way. We adopted a greedy search strategy: *backward elimination* to avoid excessive computation. This strategy suggests eliminating features one by one starting from the least promising variable. This process continued until there was solely one feature left, and the model's score for each subset was calculated by 5-fold cross-validation. The elimination of features has been done in accordance with their correlation; that is, highly correlated variables were removed initially. The cross-validation scores (CV-score) obtained for each feature subset are shown in Figure 2.8 for both datasets. The removal of the features has been done in the following order: *hf*, *mt*, *am*, *ir*, c_v, *wcr*, *pen*, and *ar*. The model used in the elimination consists of 5 hidden layers, and each of them involves 36 nodes for the A_f dataset and 30 nodes for the thermal hysteresis dataset. For the thermal hysteresis dataset, the feature subset that involves ni, ti, and ar, was selected. The selected feature subset consists of ni, ti, ar, pen, wcr, cv, ir, and am for the

Af dataset. For both datasets, adding the features hf and mt had an adverse effect on the CV error, which is the average MSE of 5 folds. This outcome justifies the redundancy of highly correlated features. The minimum CV scores for A_f and hysteresis dataset are obtained about 1.7 and 1.2.

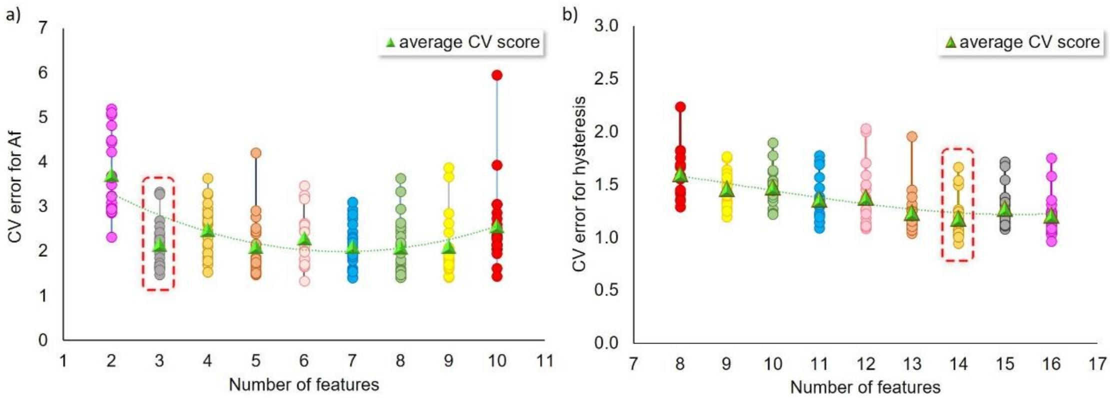

*Figure 2.8. Implementation of the wrapper methods on A_f dataset **(a)**, and thermal hysteresis dataset **(b)**. [45]*

2.4 Model optimization

For a complex model like the ANN, preventing the risk of overfitting and underfitting is crucial in terms of obtaining accurate test outcomes. Evaluation by cross-validation and optimization of the model, hence, are fundamental for a successful algorithm. Tuning of hyperparameters forms the basis of model optimization. In the current work, we put emphasis on two hyperparameters, which are the number of nodes in hidden layers and the regularization parameter. An insufficient number of nodes results in the underfitting of the model, which is easy to detect and prevent by increasing the complexity of the model. Unlike underfitting, the problem of overfitting is harder to locate since it gives low training errors despite enormous test errors. Therefore, implementing cross-validation tests is necessary to address both underfitting and overfitting problems. On the other hand, the regularization parameter primarily focuses on preventing overfitting by restricting weights. Increasing the weight of a feature raises the importance of that particular feature excessively. However, if the regularization parameter is too high, the model may underestimate the importance of the features. Therefore, selecting the optimal values of hyperparameters by trying various combinations leads the model's performance to increase significantly.

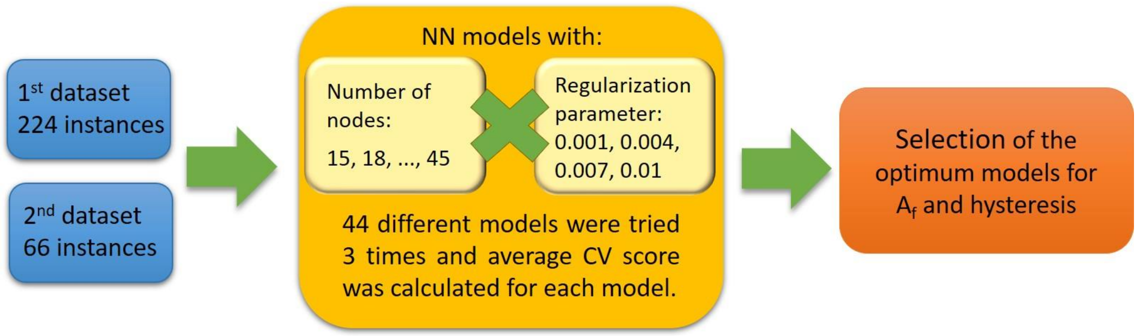

Figure 2.9. Optimal model selection chart [45]

For tuning the hyperparameters, a vast number of node and regularization parameter combinations have been tried with 5-fold cross-validation three times for both datasets, as represented in Figure 2.9. The model consisted of 5 hidden layers, and Ridge regularization was utilized due to its success in handling highly correlated features. For each combination, the average CV error was calculated and recorded. The number of nodes was selected between 15 and 45 with an increment of 3. The regularization parameter was adopted as 0.001, 0.004, 0.007, and 0.01. The CV errors of trials are supplied in Figure 2.10, where the optimum combinations are indicated with a star.

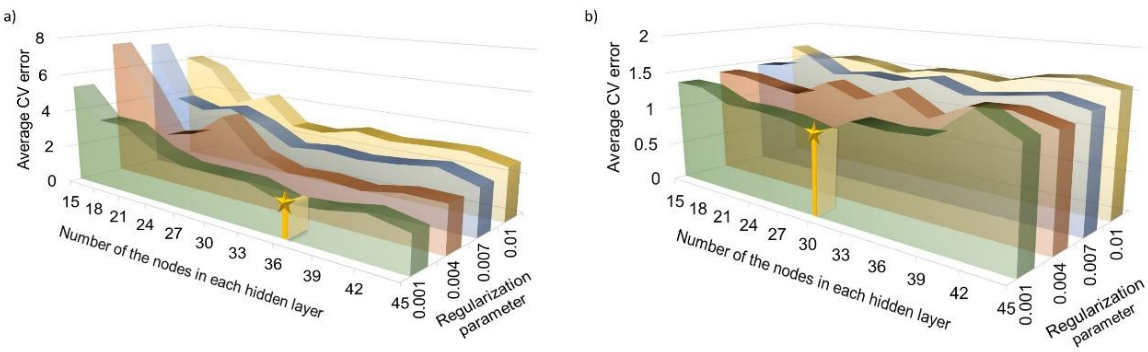

*Figure 2.10. Tuning hyperparameters of A_f dataset **(a)**, and thermal hysteresis dataset **(b)** [45]*

In Figure 2.10 (a), it is easy to observe that a lower number of nodes caused underfitting, and in Figure 2.10 (b), a higher number of nodes resulted in obvious overfitting. Also, it should be noted that, for both datasets, high regularization parameters lead the model to undervalue the features. The best result for the A_f dataset was obtained with 36 nodes in each hidden layer and the regularization parameter of 0.001. The lowest CV error was found for the thermal hysteresis dataset with 30 nodes and the same regularization parameter as in the other dataset.

2.5 *Synthetic Dataset*

The final step of designing an alloy with ML applications is predicting A_f and thermal hysteresis of undiscovered alloys. For this purpose, a search space matrix should be created, which is basically a synthetic input dataset. One integral point of the search space creation is determining the constraints of the feature, for example, trying to predict the A_f of an alloy with 10 at. % Ni content is unreliable because, in our dataset, the atomic fractions of Ni content are around 50%. Thus, one should avoid a high uncertainty range when building a synthetic dataset. By considering this, we restricted atomic fractions of Ni and Ti content between 49.5-51.5 and 20.0-48.5, respectively. The atomic fractions of both elements were increased with 0.1 increments. The atomic fraction of Hf content is evaluated by the following formula (equation (*2.9*).

$$\textit{(at. \% Hf content) = 100 - (at. \% Ni content) - (at. \% Ti content)} \tag{2.9}$$

The thermo-mechanical heat treatment variables for the thermal hysteresis dataset were selected as solution heat treatment at 1000 (C for 2 hours, one of the common thermo-mechanical treatments in the dataset. We didn't choose any aging treatment to prevent a change in alloy matrix due to precipitation. As a result, the chemical composition of the alloys is retained as the integral design parameter for prediction. The other features were calculated based on molar fractions of the components by the same methodology described in equations (2.4) and (2.5). Finally, the synthetic dataset was scaled with an identical formulation applied to the training set. As a result, the search space matrix contained 6006 different NiTiHf SMA compositions in designing new alloys.

2.6 *ML results*

The model with selected hyperparameters was utilized for training both datasets. The cost function was chosen as MSE. After training the dataset, test and training sets were saved and untransformed to obtain cost function as RMSE in the unit of degree Celsius. The distributions of predicted values with respect to actual targets for both datasets are supplied in Figure 2.11, where the diagonal line refers to the perfect fit. For the A_f model, the RMSE of the training data was calculated as 16.4 °C and the RMSE of the test data was 21.9 °C, while the R^2 parameter of the test data was 0.97. For the thermal hysteresis dataset, these scores were 11.4 °C, 11.8 °C, and 0.63, respectively. By comparing Figure 2.11 (a) and (b), one can conclude that ML managed to predict A_f values better than thermal hysteresis. It can be attributed to the relevance of features to the mechanism behind these phenomena. As mentioned before, one of the most significant factors that impact thermal hysteresis was the middle eigenvalue of B19’ to B2 transformation tensor. However, unfortunately, this variable could not be adopted in the dataset.

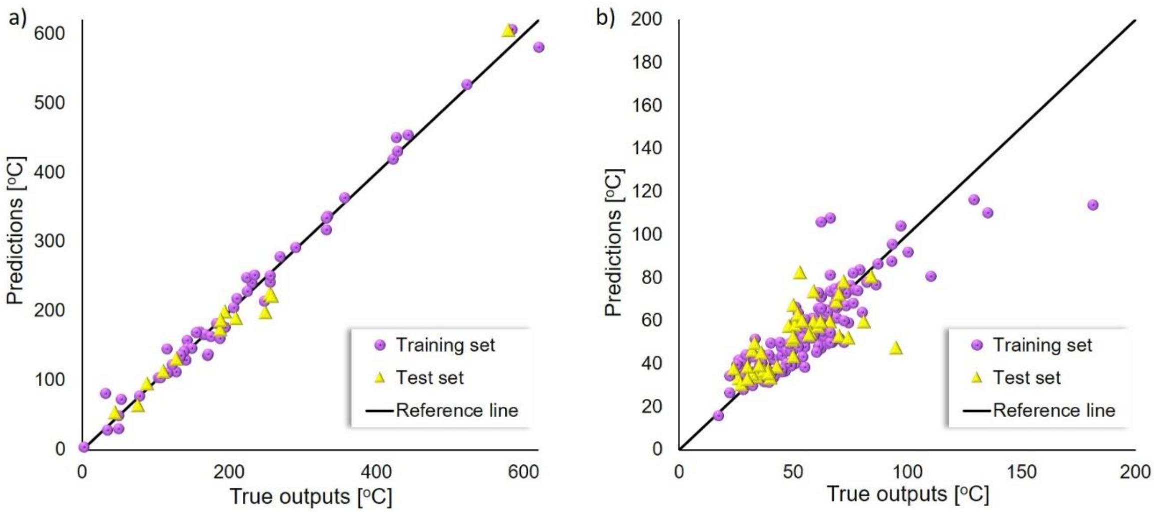

*Figure 2.11. The comparison of actual and predicted outputs of A_f dataset **(a)** and thermal hysteresis dataset **(b)** [45]*

Additionally, although the thermal hysteresis dataset showed better results in the training of the first dataset, the smallest RMSE was obtained in the second dataset for the A_f. It may be explained by the aforementioned effect of different thermo-mechanical treatments on A_f that causes A_f to be more sensitive to treatments compared to thermal hysteresis. In comparison, the thermal hysteresis is more stable with various thermo-mechanical treatments; therefore, the first dataset, which involves a higher number of data, is more suitable for the thermal hysteresis dataset.

The synthetic matrix with 6006 instances was inserted into the model to obtain Af and thermal hysteresis predictions. To figure out the relation between the targets and chemical compositions, A_f and thermal hysteresis were plotted according to Hf content and separated concerning the molar fraction of Ni in Figure 2.12. The gap between the A_f values of the alloys with 50 at.% and 50.5 at.% Ni contents demonstrates that a significant drop in TTs occurs if Ni content constitutes more than half of the molar fraction of the alloy. This phenomenon overlaps with the previous results from the experiments conducted on Ni-rich NiTiHf alloys. Additionally, A_f showed a gradual increase regarding rising Hf content, while thermal hysteresis demonstrated fluctuated response. The thermal hysteresis and the atomic fraction of Hf are almost linearly proportional if the Hf content is either less than 8 at.% or more than 25 at.%. On the contrary, the thermal hysteresis decreases as the atomic fraction of Hf inclines in the range of 11-20 at.% Hf content. A local peak of thermal hysteresis around 8-11 at.% Hf content and a local minimum around 20-25 at.% Hf content are observed. The local minimum of thermal hysteresis does not align with the previous observations found in the literature completely, mainly when the Hf content is higher than 20 at.%. However, several studies conducted on Hf-rich alloys resulted in relatively low thermal hysteresis values. Apart from this, we can intuitively deduce that the model was insufficient to comprehend the impact of Ni content on the thermal hysteresis by examining Figure 2.12 (b).

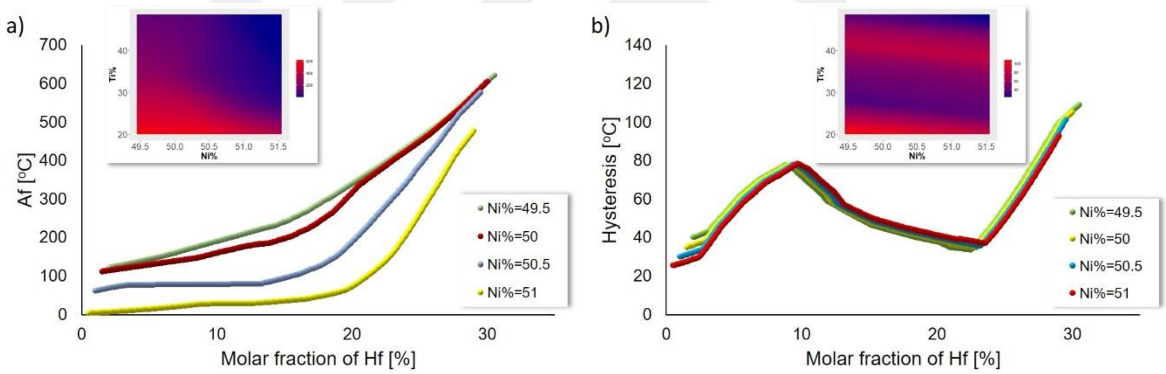

*Figure 2.12. Predictions have been made via synthetic dataset for A_f **(a)**, and thermal hysteresis **(b)** [45]*

Two compositions within the search space matrix were chosen for the validation experiments: $Ni_{49.7}Ti_{26.6}Hf_{23.7}$ and $Ni_{50}Ti_{27}Hf_{23}$. For the initial one, the A_f and thermal hysteresis were predicted as 423.6 °C and 39.4 °C, respectively. On the other hand, the latter possesses relatively lower A_f and thermal hysteresis, which are 400.6 °C and 35.9 °C, respectively. It should be emphasized that the c_v parameters of the alloys were calculated as 6.982 and 7, which occupy the high TT region defined by Zarinejad et al. [38].

2.7 References

[1] D.R. Angst, P.E. Thoma, M.Y. Kao, The Effect of Hafnium Content on the Transformation Temperatures of Ni 49 Ti 51-x Hf x . Shape Memory Alloys , J. Phys. IV. 05 (1995) C8-747-C8-752. https://doi.org/10.1051/jp4/199558747.

[2] T. Umale, D. Salas, B. Tomes, R. Arroyave, I. Karaman, The effects of wide range of compositional changes on the martensitic transformation characteristics of NiTiHf shape memory alloys, Scr. Mater. 161 (2019) 78–83. https://doi.org/10.1016/j.scriptamat.2018.10.008.

[3] J. Frenzel, A. Wieczorek, I. Opahle, B. Maaß, R. Drautz, G. Eggeler, On the effect of alloy composition on martensite start temperatures and latent heats in Ni-Ti-based shape memory alloys, Acta Mater. 90 (2015) 213–231. https://doi.org/10.1016/j.actamat.2015.02.029.

[4] H. Sehitoglu, Y. Wu, L. Patriarca, G. Li, A. Ojha, S. Zhang, Y. Chumlyakov, M. Nishida, Superelasticity and Shape Memory Behavior of NiTiHf Alloys, Shape Mem. Superelasticity. 3 (2017) 168–187. https://doi.org/10.1007/s40830-017-0108-1.

[5] S. Han, W. Zou, S. Jin, Z. Zhang, D. Yang, The Studies of the Martensite Transformations in a Ti36.5Ni48.5Hf15 Alloy, Scr. Metall. Mater. 32 (1995) 1441–1446.

[6] R. Santamarta, A. Evirgen, A.M. Perez-Sierra, J. Pons, E. Cesari, I. Karaman, R.D. Noebe, Effect of Thermal Treatments on Ni–Mn–Ga and Ni-Rich Ni–Ti–Hf/Zr High-Temperature Shape Memory Alloys, Shape Mem. Superelasticity. 1 (2015) 418–428. https://doi.org/10.1007/s40830-015-0043-y.

[7] S.M. Saghaian, H.E. Karaca, H. Tobe, A.S. Turabi, S. Saedi, S.E. Saghaian, Y.I. Chumlyakov, R.D. Noebe, High strength NiTiHf shape memory alloys with tailorable properties, Acta Mater. 134 (2017) 211–220. https://doi.org/10.1016/j.actamat.2017.05.065.

[8] S.M. Saghaian, H.E. Karaca, H. Tobe, J. Pons, R. Santamarta, Y.I. Chumlyakov, R.D. Noebe, Effects of Ni content on the shape memory properties and microstructure of Ni-rich NiTi-20Hf alloys, Smart Mater. Struct. 25 (2016) 095029. https://doi.org/10.1088/0964-1726/25/9/095029.

[9] S.M. Saghaian, H.E. Karaca, M. Souri, A.S. Turabi, R.D. Noebe, Tensile shape

memory behavior of Ni50.3Ti29.7Hf20 high temperature shape memory alloys, Mater. Des. 101 (2016) 340–345. https://doi.org/10.1016/j.matdes.2016.03.163.

[10] D. Piorunek, J. Frenzel, N. Jöns, C. Somsen, G. Eggeler, Chemical complexity, microstructure and martensitic transformation in high entropy shape memory alloys, Intermetallics. 122 (2020). https://doi.org/10.1016/j.intermet.2020.106792.

[11] L. Patriarca, H. Sehitoglu, High-temperature superelasticity of Ni50.6Ti24.4Hf25.0 shape memory alloy, Scr. Mater. 101 (2015) 12–15. https://doi.org/10.1016/j.scriptamat.2015.01.005.

[12] P. Olier, J.C. Brachet, J.L. Bechade, C. Foucher, G. Guénin, Investigation of Transformation Temperatures, Microstructure and Shape Memory Properties of NiTi, NiTiZr and NiTiHf Alloys, J. Phys. IV. 05 (1995) C8-741-C8-746. https://doi.org/10.1051/jp4/199558741.

[13] M. Moshref-Javadi, M. Belbasi, S.H. Seyedein, M.T. Salehi, Fabrication of (Ti,Hf)-rich NiTiHf Alloy Using Graphitic Mold and Crucible, J. Mater. Sci. Technol. 30 (2014) 280–284. https://doi.org/10.1016/j.jmst.2013.10.001.

[14] X.L. Meng, Y.F. Zheng, Z. Wang, L.C. Zhao, Effect of aging on the phase transformation and mechanical behavior of Ti36Ni49Hf15 high temperature shape memory alloy, Scr. Mater. 42 (2000) 341–348. https://doi.org/10.1016/S1359-6462(99)00347-4.

[15] X.L. Meng, W. Cai, Y.F. Zheng, L.C. Zhao, Phase transformation and precipitation in aged Ti-Ni-Hf high-temperature shape memory alloys, Mater. Sci. Eng. A. 438–440 (2006) 666–670. https://doi.org/10.1016/j.msea.2006.01.099.

[16] X.L. Meng, W. Cai, Y.F. Zheng, Y.X. Tong, L.C. Zhao, L.M. Zhou, Stress-induced martensitic transformation behavior of a Ti-Ni-Hf high temperature shape memory alloy, Mater. Lett. 55 (2002) 111–115. https://doi.org/10.1016/S0167-577X(01)00631-0.

[17] X.L. Meng, W. Cai, Y.D. Fu, Q.F. Li, J.X. Zhang, L.C. Zhao, Shape-memory behaviors in an aged Ni-rich TiNiHf high temperature shape-memory alloy, Intermetallics. 16 (2008) 698–705. https://doi.org/10.1016/j.intermet.2008.02.005.

[18] X.L. Meng, W. Cai, F. Chen, L.C. Zhao, Effect of aging on martensitic

transformation and microstructure in Ni-rich TiNiHf shape memory alloy, Scr. Mater. 54 (2006) 1599–1604. https://doi.org/10.1016/j.scriptamat.2006.01.017.

[19] N.A. Ley, R.W. Wheeler, O. Benafan, M.L. Young, Characterization of Thermomechanically Processed High-Temperature Ni-Lean NiTi–20 at.% Hf Shape Memory Wires, Shape Mem. Superelasticity. 5 (2019) 476–485. https://doi.org/10.1007/s40830-019-00254-1.

[20] N.A. Ley, J. Smith, R.W. Wheeler, M.L. Young, Effects of thermo-mechanical processing on precipitate evolution in Ni-rich high temperature shape memory alloys, Materialia. 8 (2019) 100496. https://doi.org/10.1016/j.mtla.2019.100496.

[21] B. Kockar, I. Karaman, J.I. Kim, Y. Chumlyakov, A method to enhance cyclic reversibility of NiTiHf high temperature shape memory alloys, Scr. Mater. 54 (2006) 2203–2208. https://doi.org/10.1016/j.scriptamat.2006.02.029.

[22] R.L. Soares, W.B. de Castro, Effects of composition on transformation temperatures and microstructure of Ni-Ti-Hf shape memory alloys, REM - Int. Eng. J. 72 (2019) 227–235. https://doi.org/10.1590/0370-44672018720072.

[23] G.S. Firstov, J. Van Humbeeck, Y.N. Koval, Comparison of high temperature shape memory behaviour for ZrCu-based, Ti-Ni-Zr and Ti-Ni-Hf alloys, Scr. Mater. 50 (2004) 243–248. https://doi.org/10.1016/j.scriptamat.2003.09.010.

[24] A.W. Young, R.W. Wheeler, N.A. Ley, O. Benafan, M.L. Young, Microstructural and Thermomechanical Comparison of Ni-Rich and Ni-Lean NiTi-20 at.% Hf High Temperature Shape Memory Alloy Wires, Shape Mem. Superelasticity. 5 (2019) 397–406. https://doi.org/10.1007/s40830-019-00255-0.

[25] A. Evirgen, F. Basner, I. Karaman, R.D. Noebe, J. Pons, R. Santamarta, Effect of aging on the martensitic transformation characteristics of a Ni-Rich NiTiHf high temperature shape memory alloy, Funct. Mater. Lett. 5 (2012) 1–5. https://doi.org/10.1142/S1793604712500385.

[26] A. Evirgen, I. Karaman, R. Santamarta, J. Pons, R.D. Noebe, Microstructural characterization and shape memory characteristics of the Ni50.3Ti34.7Hf15 shape memory alloy, Acta Mater. 83 (2015) 48–60. https://doi.org/10.1016/j.actamat.2014.09.027.

[27] G.S. Ded, Characterization of Ni-rich NiTiHf Based High Temperature Shape Memory Alloys, University of Kentucky, 2010.

[28] F. Dalle, E. Perrin, P. Vermaut, M. Masse, R. Portier, Interface mobility in Ni

49.8 Ti 42.2 Hf 8 shape memory alloy, Acta Mater. 50 (2002) 3557–3565.

[29] P.L. Potapov, A.V. Shelyakov, Effect of Hf on the structure of Ni-Ti martensitic alloys, 32 (1997) 247–250.

[30] K. Chastaing, P. Vermaut, P. Ochin, C. Segui, J.Y. Laval, R. Portier, Effect of Cu and Hf additions on NiTi martensitic transformation, Mater. Sci. Eng. A. 438–440 (2006) 661–665. https://doi.org/10.1016/j.msea.2006.02.114.

[31] D. Canadinc, W. Trehern, H. Ozcan, C. Hayrettin, O. Karakoc, I. Karaman, F. Sun, Z. Chaudhry, On the deformation response and cyclic stability of Ni50Ti35Hf15 high temperature shape memory alloy wires, Scr. Mater. 135 (2017) 92–96. https://doi.org/10.1016/j.scriptamat.2017.03.025.

[32] S. Buytoz, F. Dagdelen, I.N. Qader, M. Kok, B. Tanyildizi, Microstructure Analysis and Thermal Characteristics of NiTiHf Shape Memory Alloy with Different Composition, Met. Mater. Int. (2019). https://doi.org/10.1007/s12540-019-00444-7.

[33] A.N. Bucsek, G.A. Hudish, G.S. Bigelow, R.D. Noebe, A.P. Stebner, Composition, Compatibility, and the Functional Performances of Ternary NiTiX High-Temperature Shape Memory Alloys, Shape Mem. Superelasticity. 2 (2016) 62–79. https://doi.org/10.1007/s40830-016-0052-5.

[34] S. Besseghini, E. Villa, A. Tuissi, Ni-Ti-Hf shape memory alloy: Effect of aging and thermal cycling, Mater. Sci. Eng. A. 273–275 (1999) 390–394. https://doi.org/10.1016/s0921-5093(99)00304-4.

[35] Y. Wu, L. Patriarca, G. Li, H. Sehitoglu, Y. Soejima, T. Ito, M. Nishida, Shape Memory Response of Polycrystalline NiTi12.5Hf Alloy: Transformation at Small Scales, Shape Mem. Superelasticity. 1 (2015) 387–397. https://doi.org/10.1007/s40830-015-0033-0.

[36] O. Benafan, G.S. Bigelow, D.A. Scheiman, Transformation behavior in NiTi-20Hf shape memory alloys – Transformation temperatures and hardness, Scr. Mater. 146 (2018) 251–254. https://doi.org/10.1016/j.scriptamat.2017.11.050.

[37] O. Akgul, H.O. Tugrul, B. Kockar, Effect of the cooling rate on the thermal and thermomechanical behavior of NiTiHf high-temperature shape memory alloy, J. Mater. Res. (2020) 1–10. https://doi.org/10.1557/jmr.2020.139.

[38] M. Zarinejad, Y. Liu, Dependence of transformation temperatures of NiTi-based shape-memory alloys on the number and concentration of valence electrons, Adv.

Funct. Mater. 18 (2008) 2789–2794. https://doi.org/10.1002/adfm.200701423.

[39] Z. Zhang, J. Frenzel, K. Neuking, G. Eggeler, Vacuum induction melting of ternary NiTiX (X = Cu, Fe, Hf, Zr) shape memory alloys using graphite crucibles, Mater. Trans. 47 (2006) 661–669. https://doi.org/10.2320/matertrans.47.661.

[40] A. Evirgen, Microstructural Characterization And Shape Memory Response Of Ni-rich NiTiHf And NiTiZr High Temperature Shape Memory Alloys, Texas A&M University, 2014.

[41] Y.Q. Wang, Y.F. Zheng, W. Cai, L.C. Zhao, The Tensile Behaviour Of Ti 36 Ni 49 Hf 15 High Temperature Shape Memory Alloy, Acta Metall. 40 (1999) 1327–1331.

[42] Y. Tong, F. Chen, B. Tian, L. Li, Y. Zheng, Microstructure and martensitic transformation of Ti49Ni51−xHfx high temperature shape memory alloys, Mater. Lett. 63 (2009) 1869–1871. https://doi.org/10.1016/j.matlet.2009.05.069.

[43] P.E. Thoma, J.J. Boehm, Effect of composition on the amount of second phase and transformation temperatures of NixTi90−xHf10 shape memory alloys, Mater. Sci. Eng. A. 273–275 (1999) 385–389. https://doi.org/10.1016/S0921-5093(99)00303-2.

[44] K.S. Suresh, D.I. Kim, S.K. Bhaumik, S. Suwas, Evolution and stability of phases in a high temperature shape memory alloy Ni49.4Ti38.6Hf12, Intermetallics. 44 (2014) 18–25. https://doi.org/10.1016/j.intermet.2013.08.005.

[45] A.A. Catal, E. Bedir, R. Yilmaz, D. Canadinc, Design of a NiTiHf shape memory alloy with an austenite finish temperature beyond 400 °C utilizing artificial intelligence, J. Alloys Compd. 904 (2022) 164135. https://doi.org/10.1016/j.jallcom.2022.164135.

[46] M. Kuhn, K. Johnson, Applied Predictive Modeling, Springer New York, New York, NY, 2013. https://doi.org/10.1007/978-1-4614-6849-3.

[47] W. McKinney, Data Structures for Statistical Computing in Python, Proc. 9th Python Sci. Conf. 1 (2010) 56–61. https://doi.org/10.25080/majora-92bf1922-00a.

[48] M. Abadi, A. Agarwal, P. Barham, E. Brevdo, Z. Chen, C. Citro, G.S. Corrado, A. Davis, J. Dean, M. Devin, S. Ghemawat, I. Goodfellow, A. Harp, G. Irving, M. Isard, Y. Jia, R. Jozefowicz, L. Kaiser, M. Kudlur, J. Levenberg, D. Mane, R.

Monga, S. Moore, D. Murray, C. Olah, M. Schuster, J. Shlens, B. Steiner, I. Sutskever, K. Talwar, P. Tucker, V. Vanhoucke, V. Vasudevan, F. Viegas, O. Vinyals, P. Warden, M. Wattenberg, M. Wicke, Y. Yu, X. Zheng, TensorFlow: Large-Scale Machine Learning on Heterogeneous Distributed Systems, (2016). http://arxiv.org/abs/1603.04467.

[49] J.D. Hunter, Matplotlib: A 2D graphics environment, Comput. Sci. Eng. 9 (2007) 90–95. https://doi.org/10.1109/MCSE.2007.55.

[50] D.K. Barupal, O. Fiehn, Generating the blood exposome database using a comprehensive text mining and database fusion approach, Environ. Health Perspect. 127 (2019) 2825–2830. https://doi.org/10.1289/EHP4713.

[51] J.J. Gilman, R.W. Cumberland, R.B. Kaner, Design of hard crystals, Int. J. Refract. Met. Hard Mater. 24 (2006) 1–5. https://doi.org/10.1016/j.ijrmhm.2005.05.015.

[52] J. Ma, I. Karaman, R.D. Noebe, High temperature shape memory alloys, Int. Mater. Rev. 55 (2010) 257–315. https://doi.org/10.1179/095066010X12646898728363.

[53] J. Lee Rodgers, W. Alan Nice Wander, Thirteen ways to look at the correlation coefficient, Am. Stat. 42 (1988) 59–66. https://doi.org/10.1080/00031305.1988.10475524.

[54] R. Kohavi, H. John, Artificial Intelligence Wrappers for feature subset selection, Artif. Intell. 97 (1997) 273–324. http://linkinghub.elsevier.com/retrieve/pii/S000437029700043X.

Chapter 3:
VALIDATION EXPERIMENTS

3.1 Experimentation

The selected $Ni_{49.7}Ti_{26.6}Hf_{23.7}$ and $Ni_{50}Ti_{27}Hf_{23}$ alloys were produced by casting with Edmund-Bühler MAM-1 Vacuum Arc Melter (VAM), equipped with a water-cooled Cu crucible. The VAM was fed with Hf pellets and Ni and Ti powders with purities of 99.9, 99.7, and 99.8 wt%, respectively. While the powder size of Ni and Ti contents was within the range of 100-200 µm, the pellet size of Hf content was 1-10 mm. Initial charges of the $Ni_{49.7}Ti_{26.6}Hf_{23.7}$ and $Ni_{50}Ti_{27}Hf_{23}$ alloys were measured as 4,886 g and 4,9958 g, respectively. Prior to melting, the furnace chamber was vacuumed three times to -1 Pa pressure followed by purging Ar gas. Then, until to 0.5 bar furnace pressure, Ar gas was fed. The initial melting of Ti-alloy getter avoided the oxidation before melting of raw materials with an arc current of 4 A. The raw materials were retained in the melted stage for about 2 minutes with the average arc current of 8 A. To enhance homogeneity, melted buttons were flipped and remelted five times. The whole process has been accomplished under the condition of melting of Ti-alloy getter to entrap oxygen constantly. The casting was followed by the heat treatment of the alloys, which was conducted in a tube furnace with Ar atmosphere at 1000 °C for 2 hours and water quenching. Button specimens were cut by electrical discharge machining (EDM) to obtain disc-shaped samples with a 4 mm diameter and a 1.6 mm thickness from detected porosity and segregation-free areas of slices. The oxides and contamination owing to EDM were removed by polishing the samples with SiC emery paper in order to avoid loose contact with the thermocouples in the crucible during differential scanning calorimetry (DSC) experiments. The $Ni_{49.7}Ti_{26.6}Hf_{23.7}$ and $Ni_{50}Ti_{27}Hf_{23}$ alloys were weighted as 193.02 mg and 192.09 mg, respectively.

The TTs were investigated by a DSC experiment conducted via a NETZSCH STA 449 F3 Simultaneous Thermal Analyzer (STA). The specimens were cycled between 100 °C and 800 °C with a heating and cooling rate of 10 K/min four times under Ar atmosphere. The thermal conductivity and precise measurements were ensured by utilizing new PtRh alloy crucibles with Al_2O_3 liners and PtRh alloy lids. An 8-pureelements calibration kit (In, Sn, Bi, Zn, Al, Ag, Au, Ni) was employed to calibrate the system.

The X-ray diffraction (XRD) technique was employed to examine the phases in both SMAs via Bruker D2 Advanced X-ray diffractometer at room temperature. The device was operated at the voltage of 30 kV and the current of 10 mA with Cu-Kα radiation. The wavelength of the beam was 1.5406 Å, and the range and the speed of the 2θ angle were 15°-85°, and 2.4°/min, respectively.

3.2 *XRD Results*

The results obtained from the XRD experiment were analyzed via DIFFRAC.EVA software to find phases in the specimens. Detected peaks are displayed in Figure 3.1, where each phase is identified with the corresponding letter. Diffraction plots align with the finding of previous works that conduct experiments on Hf-rich NiTiHf SMAs [1,2]. The most widespread phase in the matrix of both alloys is the monoclinic B19’, which means that the samples are martensite at room temperature as expected. Compared to $Ni_{50}Ti_{27}Hf_{23}$ alloy, the $Ni_{49.7}Ti_{26.6}Hf_{23.7}$ alloy involves an additional orthorhombic H-phase, which causes the strengthening of the matrix and increase in thermal stabilization. This finding overlaps with our predictions, suggesting that $Ni_{49.7}Ti_{26.6}Hf_{23.7}$ alloy has higher TTs. The martensite phase continues to dominate the matrix of $Ni_{49.7}Ti_{26.6}Hf_{23.7}$ alloy after one STA cycle has been conducted; however, additional monoclinic HfO_2 and cubic precipitates of $(Ti, Hf)_2Ni$ emerged. The existence of cubic precipitates can be attributed to the temperature range of the STA cycle. During the thermal cycle, the temperatures reached almost 400 °C above the estimated value, which is 200 °C beyond the commonly applied aging temperature.

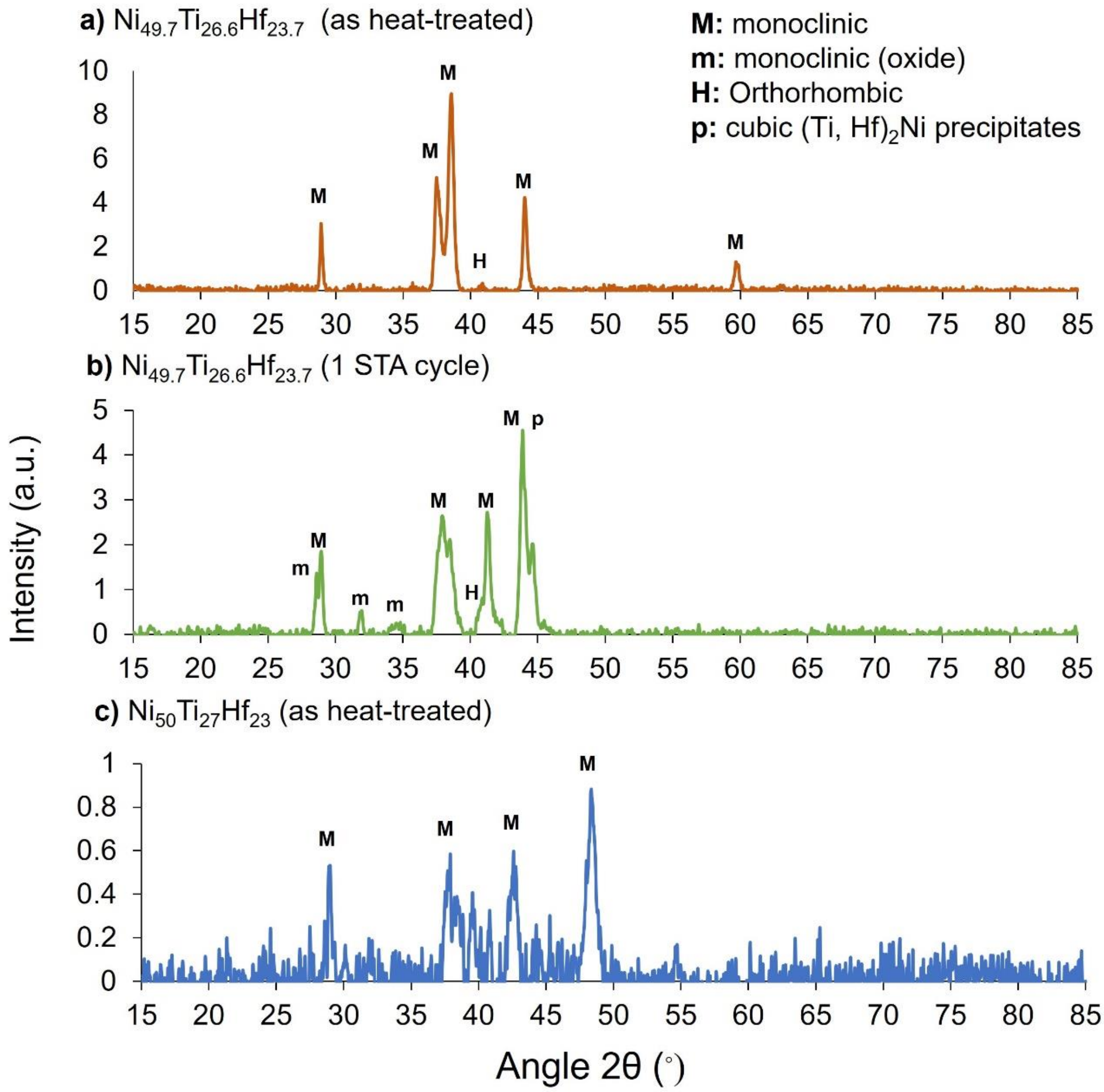

*Figure 3.1. XRD results of the as heat-treated **(a)**, stabilized $Ni_{49.7}Ti_{26.6}Hf_{23.7}$ alloy **(b)**, and $Ni_{50}Ti_{27}Hf_{23}$ alloy **(c)** [3]*

3.3 STA Results

The initial four STA cycles are demonstrated in Figure 3.2, in which the A_f and M_s temperatures are found by the intersection points of dash lines passing through the baseline and the peaks. During STA cycles, despite M_s retaining almost constant, A_f slightly decreased after the first cycle. Both endothermic and exothermic peaks have a single and sharp shape, which justifies that undesired R-phase transformation did not occur. For the $Ni_{49.7}Ti_{26.6}Hf_{23.7}$ alloy and $Ni_{50}Ti_{27}Hf_{23}$ alloy, A_f temperatures were measured as 403.5 and 308.7 °C after stabilization, respectively. M_s temperatures were found as 324.7 and 257.3 °C. Thermal hysteresis, calculated by subtracting M_s from A_f

was obtained as 78.8 °C for the $Ni_{49.7}Ti_{26.6}Hf_{23.7}$ alloy, and 51.4 °C for the $Ni_{50}Ti_{27}Hf_{23}$ alloy.

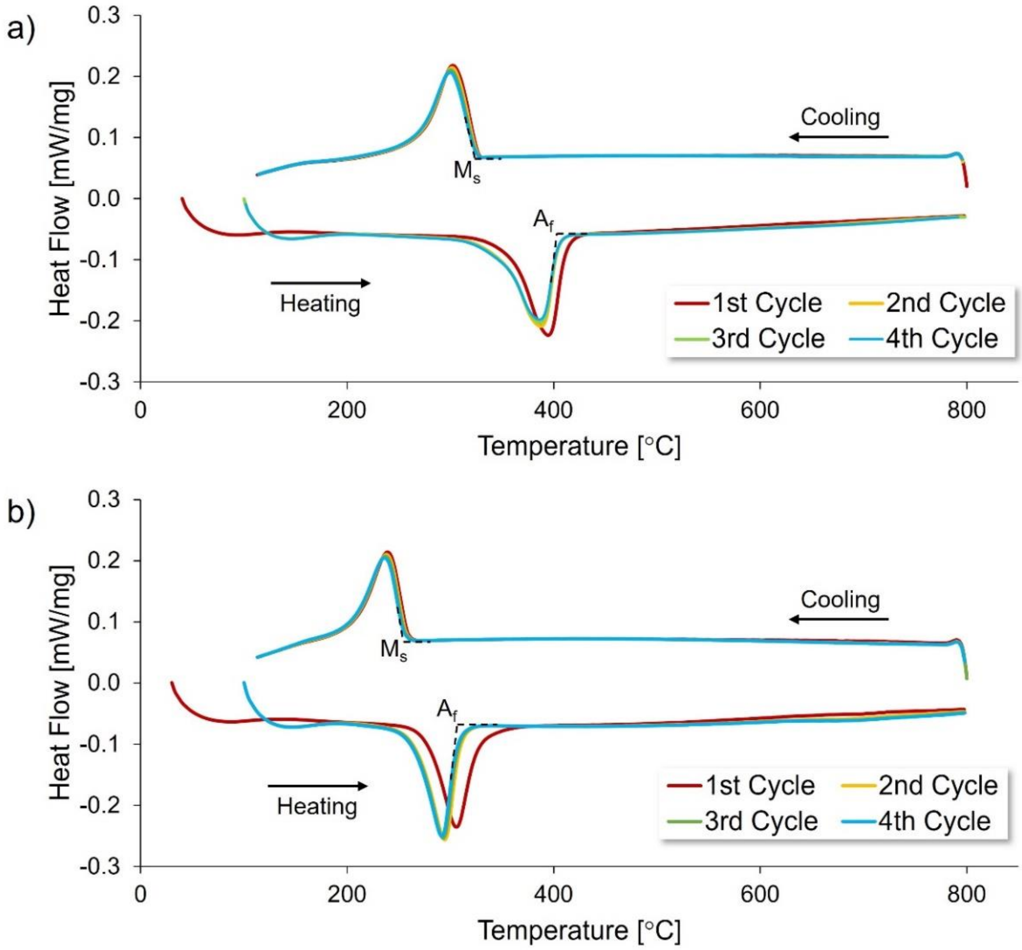

Figure 3.2. STA results of $Ni_{49.7}Ti_{26.6}Hf_{23.7}$ alloy ***(a)*** *and $Ni_{50}Ti_{27}Hf_{23}$ alloy* ***(b)*** *[3]*

A_f temperatures of both samples decreased suddenly after the initial cycle; however, they stabilized in the following cycles, as shown in Figure 3.3. Thus, we can conclude that the ML method predicted thermally stable NiTiHf with A_f temperature beyond 400 °C. Since the M_s temperature did not alter as much as A_f within thermal cycles, the thermal hysteresis dropped about 8 °C for the $Ni_{49.7}Ti_{26.6}Hf_{23.7}$ alloy and 18 °C for the $Ni_{50}Ti_{27}Hf_{23}$ alloy. The reason behind the higher stability of the $Ni_{49.7}Ti_{26.6}Hf_{23.7}$ alloy can be the H-phase found in the alloy and its high Hf content [4].

Although the ML model efficiently predicted the A_f temperature of the $Ni_{49.7}Ti_{26.6}Hf_{23.7}$ alloy, the actual output was found only about 20 °C less than the expected temperature, the stabilized hysteresis value, 78.8 °C, was measured as twice the prediction. Yet, the thermal hysteresis prediction is not disappointing since a higher error margin of the thermal hysteresis model was expected compared to the A_f model. As mentioned before, one of the critical properties that have a vital impact on thermal hysteresis, namely the middle eigenvalue of the phase transformation tensor, could not be employed as a feature because regarding information about lattice parameters was not supplied in previous studies. Moreover, in our dataset, several data show remarkably distinct thermal hysteresis values for the same composition due to different thermo-mechanical treatments; for instance, the $Ni_{50.6}Ti_{29.4}Hf_{20}$ alloy [5, 6] shows both 48 °C and 93 °C depending on applied treatments. Therefore, one can conclude that the alloy's microstructure, which is highly sensitive to applied thermo-mechanical treatment, affects the thermal hysteresis. As a result, the thermal hysteresis values of the alloys in the current study may hopefully be improved by suitable treatments.

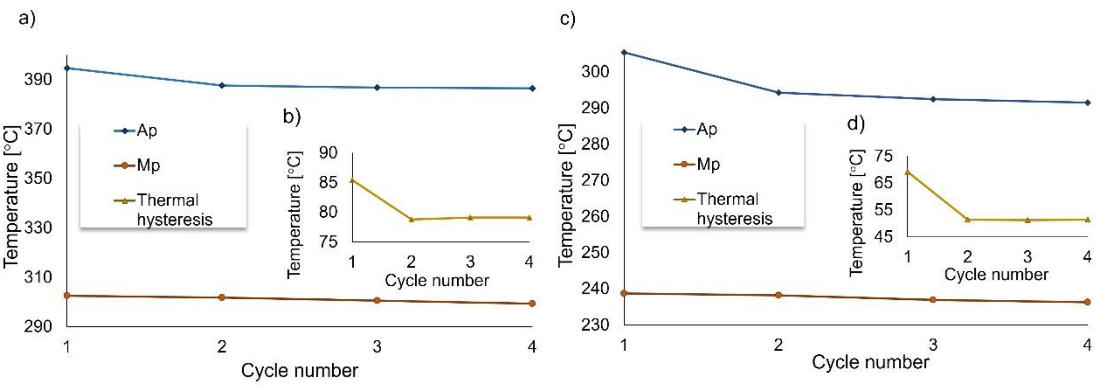

*Figure 3.3. A_p, M_p, and thermal hysteresis graph of $Ni_{49.7}Ti_{26.6}Hf_{23.7}$ alloy **(a)** and $Ni_{50}Ti_{27}Hf_{23}$ alloy **(b)** [3]*

By comparison to the $Ni_{49.7}Ti_{26.6}Hf_{23.7}$ alloy, the STA experiment of the $Ni_{50}Ti_{27}Hf_{23}$ alloy resulted in highly different from the predicted value. Even though the $Ni_{50}Ti_{27}Hf_{23}$ alloy was expected to have an A_f of 400.6 °C, the actual outcome obtained by the validation experiment was 91.9 °C less than the prediction. This result is unexpected because its average valence electron number is the desired value, 7. Additionally, the substitution of Hf for Ti is expected to raise A_f temperature; however, the $Ni_{50}Ti_{30}Hf_{20}$ alloy in our dataset has a higher A_f temperature than the selected alloy. This circumstance can be explained by the non-overlapping actual and nominal chemical compositions either in selected alloy or available literature data used for training. The disparity of actual and nominal compositions originates from precipitation in the matrix, which also affects TTs. To overcome this problem, the dataset should contain the composition of the actual matrix or microstructural details, such as precipitate size and volume fraction.

3.4 References

[1] R.L. Soares, W.B. de Castro, Effects of composition on transformation temperatures and microstructure of Ni-Ti-Hf shape memory alloys, REM - Int. Eng. J. 72 (2019) 227–235. https://doi.org/10.1590/0370-44672018720072.

[2] D.H.D. Hsu, Design and development of NiTi-based precipitation-strengthened high-temperature shape memory alloys for actuator applications, 2013. https://www.proquest.com/dissertations-theses/design-development-niti-based-precipitation/docview/1774013699/se-2?accountid=8359%0Ahttp://ne4ke2fg4p.search.serialssolutions.com/directLink?&atitle=Design+and+development+of+NiTi-based+precipitation-strength.

[3] A.A. Catal, E. Bedir, R. Yilmaz, D. Canadinc, Design of a NiTiHf shape memory alloy with an austenite finish temperature beyond 400 °C utilizing artificial intelligence, J. Alloys Compd. 904 (2022) 164135. https://doi.org/10.1016/j.jallcom.2022.164135.

[4] A. Evirgen, J. Pons, I. Karaman, R. Santamarta, R.D. Noebe, H-Phase Precipitation and Martensitic Transformation in Ni-rich Ni–Ti–Hf and Ni–Ti-Zr High-Temperature Shape Memory Alloys, Shape Mem. Superelasticity. 4 (2018) 85–92. https://doi.org/10.1007/s40830-018-0165-0.

[5] X.L. Meng, W. Cai, Y.F. Zheng, L.C. Zhao, Phase transformation and precipitation in aged Ti-Ni-Hf high-temperature shape memory alloys, Mater. Sci. Eng. A. 438–440 (2006) 666–670. https://doi.org/10.1016/j.msea.2006.01.099.

[6] X.L. Meng, W. Cai, Y.D. Fu, Q.F. Li, J.X. Zhang, L.C. Zhao, Shape-memory behaviors in an aged Ni-rich TiNiHf high temperature shape-memory alloy, Intermetallics. 16 (2008) 698–705. https://doi.org/10.1016/j.intermet.2008.02.005.

Chapter 4:
CONCLUSIONS AND FUTURE WORK

NiTiHf high-temperature shape memory alloys have drawn tremendous interest owing to their high operating temperature range, medium-ductility, and notably lower cost among various high-temperature shape memory alloy systems. Increasing demand in the aerospace and oil industry encourages the search for optimal NiTiHf alloy. Machine learning application in material science promised affordable alloy design methodology recently, which led us to integrate ML algorithms to optimal NiTiHf search. The main goal was designing a NiTiHf alloy that can exhibit martensite to austenite phase transformation beyond 400 ℃, with relatively low thermal hysteresis.

To accomplish this, a multilayer feedforward neural network was established and utilized to learn from the available literature on NiTiHf alloy. The neural network model was optimized by determining the feature set via wrapper method and tuning the number of nodes and regularization parameter via trial-and-error. Then, a search space matrix was built for the prediction of new compositions. Two compositions with desired functions, the $Ni_{49.7}Ti_{26.6}Hf_{23.7}$, and the $Ni_{50}Ti_{27}Hf_{23}$ alloys, were utilized to validate machine learning predictions. While $Ni_{50}Ti_{27}Hf_{23}$ could not reach 400 ℃, the $Ni_{49.7}Ti_{26.6}Hf_{23.7}$ demonstrated high cyclic stability with an A_f temperature of 403.5 °C. To enhance the model's performance, systematic research on the microstructure of available NiTiHf data should be conducted in the future. Especially, their actual chemical composition, lattice parameters in austenite and martensite phases, and precipitations are required to be investigated in detail. With this additional effort and our alloy designing methodology based on a neural network algorithm, the discovery of new NiTiHf alloys will hopefully accelerate.

Appendix A: Datasets

Table 0.1. Chemical properties of the elements that form the alloy

	Ni	Ti	Hf
Valence electron number	10	4	4
Atomic number	28	22	72
Atomic radius [nm]	0.125	0.147	0.159
Ionic radius [nm]	0.078	0.076	0.084
Waber-Cromer's radius [Å]	0.339	0.468	0.829
Electronegativity	1.91	1.54	1.3
Atomic mass [amu]	58.71	47.9	178.49
Melting point [°C]	1455	1670	2231

*Table 0.2. First Dataset**

ref.	Ni [at.%]	Ti [at.%]	Hf [at.%]	Cv	Calculated melting point* [°C]	Calculated electro-negativity	Calculated atomic radius [nm]	Calculated ionic radius [nm]	Calculated atomic mass [amu]	Calculated Waber-Cromer's pseudo-potential radius [Å]	Homogenization		Solution heat treatment		Aging treatment		A_f [°C]	Thermal hysteresis [°C]
											Temperature [°C]	Time [h]	Temperature [°C]	Time [h]	Temperature [°C]	Time [h]		
[31]	50	35	15	0.2154	1646.7	1.6890	0.1378	0.0782	72.894	0.458	0	0	0	0	0	0	220	70
[21]	49.8	42.2	8	0.2411	1607.8	1.7051	0.1370	0.0776	63.731	0.435	1000	24	0	0	0	0	165	64.3
[25]	50.3	34.7	15	0.2158	1646.0	1.6901	0.1377	0.0782	72.926	0.458	1050	72	900	1	600	1	127	60
[25]	50.3	34.7	15	0.2158	1646.0	1.6901	0.1377	0.0782	72.926	0.458	1050	72	900	1	600	3	156	61
[25]	50.3	34.7	15	0.2158	1646.0	1.6901	0.1377	0.0782	72.926	0.458	1050	72	900	1	600	48	165	62
[25]	50.3	34.7	15	0.2158	1646.0	1.6901	0.1377	0.0782	72.926	0.458	1050	72	900	1	600	24	165	63
[25]	50.3	34.7	15	0.2158	1646.0	1.6901	0.1377	0.0782	72.926	0.458	1050	72	900	1	0	0	83	73
[14]	49	36	15	0.2139	1648.8	1.6853	0.1380	0.0782	72.785	0.460	950	1.5	1000	1	700	5	210	59
[14]	49	36	15	0.2139	1648.8	1.6853	0.1380	0.0782	72.785	0.460	950	1.5	1000	1	700	10	190	66
[14]	49	36	15	0.2139	1648.8	1.6853	0.1380	0.0782	72.785	0.460	950	1.5	1000	1	700	20	195	68
[14]	49	36	15	0.2139	1648.8	1.6853	0.1380	0.0782	72.785	0.460	950	1.5	1000	1	700	120	192	70
[41]	49	36	15	0.2139	1648.8	1.6853	0.1380	0.0782	72.785	0.460	950	1.5	900	1	0	0	231	52
[33]	50.3	25.6	24.1	0.1893	1697.1	1.6683	0.1388	0.0789	84.810	0.488	1050	72	0	0	500	100	291	34
[17]	50.6	29.4	20	0.2008	1673.4	1.6792	0.1383	0.0786	79.488	0.474	950	4	950	4	0	0	174	53
[17]	50.6	29.4	20	0.2008	1673.4	1.6792	0.1383	0.0786	79.488	0.474	950	4	950	4	550	2	315	93
[9]	50.3	29.7	20	0.2004	1674.1	1.6781	0.1383	0.0786	79.455	0.475	1050	72	0	0	800	3	129	35
[34]	50	40	10	0.2333	1618.6	1.7010	0.1372	0.0778	66.364	0.441	0	0	900	1	900	1	193	69
[34]	50	40	10	0.2333	1618.6	1.7010	0.1372	0.0778	66.364	0.441	0	0	900	1	0	0	198	70
[34]	50	40	10	0.2333	1618.6	1.7010	0.1372	0.0778	66.364	0.441	0	0	900	1	400	1	187	71
[34]	50	40	10	0.2333	1618.6	1.7010	0.1372	0.0778	66.364	0.441	0	0	900	1	600	1	210	86
[34]	49	41	10	0.2318	1620.8	1.6973	0.1374	0.0778	66.256	0.443	0	0	900	1	0	0	194	64
[34]	49	41	10	0.2318	1620.8	1.6973	0.1374	0.0778	66.256	0.443	0	0	900	1	800	1	191	68

[34]	40	50	10	0.2177	1640.1	1.6640	0.1394	0.0776	65.283	0.457	0	0	900	1	0	0	212	63
[28]	49.8	42.2	8	0.2411	1607.8	1.7051	0.1370	0.0776	63.731	0.435	800	60	0	0	0	0	177	80
[8]	52	28	20	0.2027	1670.4	1.6844	0.1380	0.0786	79.639	0.472	1000	48	0	0	0	0	160	60
[8]	51.2	28.8	20	0.2016	1672.1	1.6814	0.1381	0.0786	79.553	0.473	1000	48	0	0	0	0	197	66
[8]	50.7	29.3	20	0.2010	1673.2	1.6796	0.1382	0.0786	79.499	0.474	1000	48	0	0	0	0	137	26
[8]	50.3	29.7	20	0.2004	1674.1	1.6781	0.1383	0.0786	79.455	0.475	1000	48	0	0	0	0	189	33
[4]	50.5	36.2	13.3	0.2219	1636.0	1.6949	0.1375	0.0781	70.728	0.451	0	0	0	0	0	0	31.2	62.9
[4]	50.3	25	24.7	0.1878	1700.4	1.6668	0.1389	0.0790	85.593	0.490	0	0	0	0	0	0	422	82
[26]	50.3	34.7	15	0.2158	1646.0	1.6901	0.1377	0.0782	72.926	0.458	1050	72	900	1	550	1	98	51
[26]	50.3	34.7	15	0.2158	1646.0	1.6901	0.1377	0.0782	72.926	0.458	1050	72	900	1	550	24	113	53
[26]	50.3	34.7	15	0.2158	1646.0	1.6901	0.1377	0.0782	72.926	0.458	1050	72	900	1	500	24	87	53
[26]	50.3	34.7	15	0.2158	1646.0	1.6901	0.1377	0.0782	72.926	0.458	1050	72	900	1	550	48	121	54
[26]	50.3	34.7	15	0.2158	1646.0	1.6901	0.1377	0.0782	72.926	0.458	1050	72	900	1	500	48	96	54
[26]	50.3	34.7	15	0.2158	1646.0	1.6901	0.1377	0.0782	72.926	0.458	1050	72	900	1	550	10	111	55
[26]	50.3	34.7	15	0.2158	1646.0	1.6901	0.1377	0.0782	72.926	0.458	1050	72	900	1	500	10	76	56
[26]	50.3	34.7	15	0.2158	1646.0	1.6901	0.1377	0.0782	72.926	0.458	1050	72	900	1	450	24	50	57
[26]	50.3	34.7	15	0.2158	1646.0	1.6901	0.1377	0.0782	72.926	0.458	1050	72	900	1	450	48	48	59
[26]	50.3	34.7	15	0.2158	1646.0	1.6901	0.1377	0.0782	72.926	0.458	1050	72	900	1	500	1	51	62
[26]	50.3	34.7	15	0.2158	1646.0	1.6901	0.1377	0.0782	72.926	0.458	1050	72	900	1	450	3	29	74
[26]	50.3	34.7	15	0.2158	1646.0	1.6901	0.1377	0.0782	72.926	0.458	1050	72	900	1	450	1	42	81
[18]	49	41	10	0.2318	1620.8	1.6973	0.1374	0.0778	66.256	0.443	0	0	0	0	0	0	185	62
[13]	49	36	15	0.2139	1648.8	1.6853	0.1380	0.0782	72.785	0.460	0	0	0	0	0	0	221	51
[39]	49.5	35.5	15	0.2147	1647.7	1.6872	0.1379	0.0782	72.839	0.459	1000	30	0	0	0	0	254	44
[39]	49.5	35.5	15	0.2147	1647.7	1.6872	0.1379	0.0782	72.839	0.459	0	0	0	0	0	0	254.8	49.3
[38]	40	50	10	0.2177	1640.1	1.6640	0.1394	0.0776	65.283	0.457	0	0	0	0	0	0	205	65
[38]	35	50	15	0.1930	1678.9	1.6335	0.1411	0.0779	71.272	0.483	0	0	0	0	0	0	290	55
[29]	49.8	35.2	15	0.2151	1647.1	1.6883	0.1378	0.0782	72.872	0.458	0	0	0	0	0	0	210	74
[29]	49.8	39.2	11	0.2292	1624.6	1.6979	0.1374	0.0779	67.648	0.445	0	0	0	0	0	0	182	59

[29]	49.8	40.7	9.5	0.2350	1616.2	1.7015	0.1372	0.0778	65.689	0.440	0	0	0	0	0	0	159	69
[29]	49.8	42.2	8	0.2411	1607.8	1.7051	0.1370	0.0776	63.731	0.435	0	0	0	0	0	0	142	73
[6]	50.1	24.9	25	0.1868	1702.5	1.6654	0.1390	0.0790	85.963	0.492	0	0	0	0	550	3	273	97
[24]	50.8	29.2	20	0.2011	1673.0	1.6800	0.1382	0.0786	79.509	0.474	1050	72	1050	3	775	0.5	124	32
[24]	50.8	29.2	20	0.2011	1673.0	1.6800	0.1382	0.0786	79.509	0.474	1050	72	1050	3	800	0.5	110	32
[24]	50.8	29.2	20	0.2011	1673.0	1.6800	0.1382	0.0786	79.509	0.474	1050	72	0	0	0	0	110	33
[24]	50.8	29.2	20	0.2011	1673.0	1.6800	0.1382	0.0786	79.509	0.474	1050	72	1050	3	825	0.5	110	34
[24]	50.8	29.2	20	0.2011	1673.0	1.6800	0.1382	0.0786	79.509	0.474	1050	72	1050	3	750	0.5	148	35
[24]	50.8	29.2	20	0.2011	1673.0	1.6800	0.1382	0.0786	79.509	0.474	1050	72	1050	3	725	0.5	174	42
[19]	49.8	30.2	20	0.1997	1675.1	1.6763	0.1384	0.0786	79.401	0.475	1050	72	0	0	0	0	331	46.4
[18]	50	30	20	0.2000	1674.7	1.6770	0.1384	0.0786	79.423	0.475	1000	4	900	1	0	0	309	69
[12]	50	38	12	0.2258	1629.8	1.6962	0.1374	0.0780	68.976	0.448	900	48	0	0	0	0	194	52
[5]	48.5	36.5	15	0.2132	1649.9	1.6835	0.1381	0.0782	72.731	0.460	1000	11	0	0	500	1	255	55
[15]	50.8	29.2	20	0.2011	1673.0	1.6800	0.1382	0.0786	79.509	0.474	1000	4	900	1	550	2	127	76
[15]	50.6	29.4	20	0.2008	1673.4	1.6792	0.1383	0.0786	79.488	0.474	1000	4	900	1	550	30	295	48
[15]	50.6	29.4	20	0.2008	1673.4	1.6792	0.1383	0.0786	79.488	0.474	1000	4	900	1	550	1	210	66
[15]	50.6	29.4	20	0.2008	1673.4	1.6792	0.1383	0.0786	79.488	0.474	1000	4	900	1	550	5	317	72
[15]	50.6	29.4	20	0.2008	1673.4	1.6792	0.1383	0.0786	79.488	0.474	1000	4	900	1	0	0	157	78
[15]	50.6	29.4	20	0.2008	1673.4	1.6792	0.1383	0.0786	79.488	0.474	1000	4	900	1	550	2	308	84
[23]	49.42	35.95	14.63	0.2158	1645.8	1.6877	0.1379	0.0782	72.348	0.458	0	0	0	0	0	0	230	54
[43]	49.8	40.2	10	0.2330	1619.0	1.7003	0.1372	0.0778	66.342	0.441	900	100	0	0	0	0	199	73
[30]	49.8	40.2	10	0.2330	1619.0	1.7003	0.1372	0.0778	66.342	0.441	800	1	0	0	0	0	173	55
[10]	50	25	25	0.1867	1702.8	1.6650	0.1390	0.0790	85.953	0.492	900	100	0	0	0	0	441.4	17.2
[3]	49.8	30.2	20	0.1997	1675.1	1.6763	0.1384	0.0786	79.401	0.475	950	72	0	0	0	0	337.6	37.5
[3]	49.8	35.2	15	0.2151	1647.1	1.6883	0.1378	0.0782	72.872	0.458	950	72	0	0	0	0	257.9	50.9
[3]	49.8	39.2	11	0.2292	1624.6	1.6979	0.1374	0.0779	67.648	0.445	950	72	0	0	0	0	202.9	61
[3]	49.8	40.2	10	0.2330	1619.0	1.7003	0.1372	0.0778	66.342	0.441	950	72	0	0	0	0	191.8	63.7
[3]	49.8	42.2	8	0.2411	1607.8	1.7051	0.1370	0.0776	63.731	0.435	950	72	0	0	0	0	175.3	64.2

[3]	49.8	44.2	6	0.2497	1596.6	1.7099	0.1368	0.0775	61.119	0.428	950	72	0	0	0	0	148.4	57.5
[3]	49.8	46.2	4	0.2589	1585.4	1.7147	0.1365	0.0773	58.507	0.421	950	72	0	0	0	0	133.8	48
[3]	49.8	48.2	2	0.2689	1574.2	1.7195	0.1363	0.0772	55.895	0.414	950	72	0	0	0	0	121.7	39.1
[7]	51.2	28.8	20	0.2016	1672.1	1.6814	0.1381	0.0786	79.553	0.473	1000	48	900	3	600	3	134	51
[7]	51.2	28.8	20	0.2016	1672.1	1.6814	0.1381	0.0786	79.553	0.473	1000	48	900	3	650	3	153	53
[7]	51.2	28.8	20	0.2016	1672.1	1.6814	0.1381	0.0786	79.553	0.473	1000	48	900	3	700	3	150	60
[7]	51.2	28.8	20	0.2016	1672.1	1.6814	0.1381	0.0786	79.553	0.473	1000	48	900	3	550	3	93	61
[7]	51.2	28.8	20	0.2016	1672.1	1.6814	0.1381	0.0786	79.553	0.473	1000	48	900	3	750	3	125	62
[20]	50.5	34.5	15	0.2161	1645.6	1.6909	0.1377	0.0782	72.948	0.457	1050	1	0	0	550	3	131	22
[20]	50.5	34.5	15	0.2161	1645.6	1.6909	0.1377	0.0782	72.948	0.457	1050	1	0	0	0	0	88	36
[20]	50.5	34.5	15	0.2161	1645.6	1.6909	0.1377	0.0782	72.948	0.457	1050	1	0	0	750	3	127	38.8
[35]	51	36.5	12.5	0.2255	1630.5	1.6987	0.1373	0.0780	69.737	0.448	1000	4	0	0	0	0	54	54
[35]	51	36.5	12.5	0.2255	1630.5	1.6987	0.1373	0.0780	69.737	0.448	1000	4	900	1	637	11	71	59
[35]	51	36.5	12.5	0.2255	1630.5	1.6987	0.1373	0.0780	69.737	0.448	1000	4	900	1	605	4	49	66
[35]	51	36.5	12.5	0.2255	1630.5	1.6987	0.1373	0.0780	69.737	0.448	1000	4	900	1	665	4	53	69
[35]	51	36.5	12.5	0.2255	1630.5	1.6987	0.1373	0.0780	69.737	0.448	1000	4	900	1	637	1	24	72
[35]	51	36.5	12.5	0.2255	1630.5	1.6987	0.1373	0.0780	69.737	0.448	1000	4	900	1	637	100	111	77
[37]	50	30	20	0.2000	1674.7	1.6770	0.1384	0.0786	79.423	0.475	0	0	0	0	0	0	331	45
[22]	50	33	17	0.2090	1657.9	1.6842	0.1380	0.0784	75.505	0.465	0	0	0	0	0	0	224.31	44.53
[22]	50	36	14	0.2188	1641.0	1.6914	0.1377	0.0781	71.588	0.455	0	0	0	0	0	0	188.1	56.12
[22]	50	39	11	0.2295	1624.2	1.6986	0.1373	0.0779	67.670	0.444	0	0	0	0	0	0	154.45	60.9
[22]	50	42	8	0.2414	1607.4	1.7058	0.1370	0.0776	63.752	0.434	0	0	0	0	0	0	115	69.42
[17]	51	19	30	0.1762	1728.7	1.6567	0.1394	0.0794	92.590	0.507	0	0	1050	2	0	0	522	129
[17]	51	24	25	0.1880	1700.6	1.6687	0.1388	0.0790	86.061	0.490	0	0	1050	2	0	0	186	33
[17]	51	29	20	0.2014	1672.6	1.6807	0.1382	0.0786	79.531	0.473	0	0	1050	2	0	0	53	49
[17]	51	49	0	0.2817	1560.4	1.7287	0.1358	0.0770	53.413	0.405	0	0	1050	2	0	0	2	22
[17]	50.7	19.3	30	0.1759	1729.3	1.6556	0.1394	0.0794	92.558	0.508	0	0	1050	2	0	0	620	181
[17]	50.7	24.3	25	0.1876	1701.2	1.6676	0.1388	0.0790	86.028	0.491	0	0	1050	2	0	0	333	72

[17]	50.7	29.3	20	0.2010	1673.2	1.6796	0.1382	0.0786	79.499	0.474	0	0	1050	2	0	0	171	28
[17]	50.7	34.3	15	0.2164	1645.1	1.6916	0.1376	0.0782	72.969	0.457	0	0	1050	2	0	0	76	50
[17]	50.7	39.3	10	0.2344	1617.1	1.7036	0.1370	0.0778	66.440	0.440	0	0	1050	2	0	0	45	110
[17]	50.7	44.3	5	0.2557	1589.0	1.7156	0.1364	0.0774	59.910	0.423	0	0	1050	2	0	0	49	58
[17]	50.7	49.3	0	0.2812	1561.0	1.7276	0.1358	0.0770	53.381	0.406	0	0	1050	2	0	0	34	28
[17]	50.3	19.7	30	0.1754	1730.2	1.6541	0.1395	0.0794	92.514	0.509	0	0	1050	2	0	0	622	135
[17]	50.3	24.7	25	0.1871	1702.1	1.6661	0.1389	0.0790	85.985	0.492	0	0	1050	2	0	0	428	95
[17]	50.3	29.7	20	0.2004	1674.1	1.6781	0.1383	0.0786	79.455	0.475	0	0	1050	2	0	0	289	32
[17]	50.3	34.7	15	0.2158	1646.0	1.6901	0.1377	0.0782	72.926	0.458	0	0	1050	2	0	0	183	40
[17]	50.3	39.7	10	0.2338	1618.0	1.7021	0.1371	0.0778	66.396	0.441	0	0	1050	2	0	0	127	75
[17]	50.3	44.7	5	0.2550	1589.9	1.7141	0.1365	0.0774	59.867	0.424	0	0	1050	2	0	0	103	62
[17]	50.3	49.7	0	0.2805	1561.9	1.7261	0.1359	0.0770	53.337	0.407	0	0	1050	2	0	0	78	32
[17]	50	20	30	0.1750	1730.8	1.6530	0.1396	0.0794	92.482	0.509	0	0	1050	2	0	0	583	66
[17]	50	25	25	0.1867	1702.8	1.6650	0.1390	0.0790	85.953	0.492	0	0	1050	2	0	0	426	48
[17]	50	30	20	0.2000	1674.7	1.6770	0.1384	0.0786	79.423	0.475	0	0	1050	2	0	0	335	37
[17]	50	35	15	0.2154	1646.7	1.6890	0.1378	0.0782	72.894	0.458	0	0	1050	2	0	0	249	45
[17]	50	40	10	0.2333	1618.6	1.7010	0.1372	0.0778	66.364	0.441	0	0	1050	2	0	0	187	61
[17]	50	45	5	0.2545	1590.6	1.7130	0.1366	0.0774	59.835	0.424	0	0	1050	2	0	0	141	54
[17]	50	50	0	0.2800	1562.5	1.7250	0.1360	0.0770	53.305	0.407	0	0	1050	2	0	0	106	37
[17]	49.8	20.2	30	0.1748	1731.2	1.6523	0.1396	0.0794	92.460	0.509	0	0	1050	2	0	0	579	62
[17]	49.8	25.2	25	0.1864	1703.2	1.6643	0.1390	0.0790	85.931	0.492	0	0	1050	2	0	0	442	36
[17]	49.8	30.2	20	0.1997	1675.1	1.6763	0.1384	0.0786	79.401	0.475	0	0	1050	2	0	0	337	31
[17]	49.8	35.2	15	0.2151	1647.1	1.6883	0.1378	0.0782	72.872	0.458	0	0	1050	2	0	0	244	50
[17]	49.8	40.2	10	0.2330	1619.0	1.7003	0.1372	0.0778	66.342	0.441	0	0	1050	2	0	0	188	62
[17]	49.8	45.2	5	0.2542	1591.0	1.7123	0.1366	0.0774	59.813	0.424	0	0	1050	2	0	0	137.6	58
[17]	49.8	50.2	0	0.2797	1562.9	1.7243	0.1360	0.0770	53.283	0.407	0	0	1050	2	0	0	115.3	32
[11]	50.6	24.4	25	0.1874	1701.5	1.6672	0.1389	0.0790	86.017	0.491	1000	4	900	1	500	4	275	29
[11]	50.6	24.4	25	0.1874	1701.5	1.6672	0.1389	0.0790	86.017	0.491	1000	4	900	1	500	1	261	34

[11]	50.6	24.4	25	0.1874	1701.5	1.6672	0.1389	0.0790	86.017	0.491	1000	4	900	1	400	4	238	45
[11]	50.6	24.4	25	0.1874	1701.5	1.6672	0.1389	0.0790	86.017	0.491	1000	4	900	1	600	4	337	50
[11]	50.6	24.4	25	0.1874	1701.5	1.6672	0.1389	0.0790	86.017	0.491	1000	4	900	1	0	0	272	52
[11]	50.6	24.4	25	0.1874	1701.5	1.6672	0.1389	0.0790	86.017	0.491	1000	4	900	1	700	4	356	66
[11]	50.6	24.4	25	0.1874	1701.5	1.6672	0.1389	0.0790	86.017	0.491	1000	4	0	0	0	0	369	68
[44]	49.4	38.6	12	0.2249	1631.1	1.6940	0.1376	0.0779	68.911	0.449	0	0	1000	24	900	1	240	50
[44]	49.4	38.6	12	0.2249	1631.1	1.6940	0.1376	0.0779	68.911	0.449	0	0	0	0	0	0	247	52
[44]	49.4	38.6	12	0.2249	1631.1	1.6940	0.1376	0.0779	68.911	0.449	0	0	1000	24	0	0	285	87
[32]	27	70	3	0.2237	1628.8	1.6327	0.1414	0.0768	54.736	0.455	0	0	0	0	0	0	132.4	93.2
[32]	24	70	6	0.2057	1652.1	1.6144	0.1424	0.0770	58.330	0.470	0	0	0	0	0	0	164.6	100
[32]	21	70	9	0.1895	1675.3	1.5961	0.1435	0.0771	61.923	0.485	0	0	0	0	0	0	254.7	78.9
[42]	49	36	15	0.2139	1648.8	1.6853	0.1380	0.0782	72.785	0.460	900	5	0	0	0	0	343	62
[42]	49	41	10	0.2318	1620.8	1.6973	0.1374	0.0778	66.256	0.443	900	5	0	0	0	0	220	65
[42]	49	44	7	0.2440	1603.9	1.7045	0.1371	0.0775	62.338	0.432	900	5	0	0	0	0	167	76
[42]	49	46	5	0.2529	1592.7	1.7093	0.1368	0.0774	59.726	0.426	900	5	0	0	0	0	142	62
[42]	49	48	3	0.2625	1581.5	1.7141	0.1366	0.0772	57.115	0.419	900	5	0	0	0	0	128	52
[36]	51	29	20	0.2014	1672.6	1.6807	0.1382	0.0786	79.531	0.473	1050	72	0	0	650	3	183	59
[36]	51	29	20	0.2014	1672.6	1.6807	0.1382	0.0786	79.531	0.473	1050	72	0	0	0	0	208	63
[36]	51	29	20	0.2014	1672.6	1.6807	0.1382	0.0786	79.531	0.473	1050	72	0	0	400	3	212	65
[36]	51	29	20	0.2014	1672.6	1.6807	0.1382	0.0786	79.531	0.473	1050	72	0	0	550	3	219	70
[36]	50.9	29.1	20	0.2012	1672.8	1.6803	0.1382	0.0786	79.520	0.474	1050	72	0	0	650	3	184	58
[36]	50.9	29.1	20	0.2012	1672.8	1.6803	0.1382	0.0786	79.520	0.474	1050	72	0	0	400	3	209	62
[36]	50.9	29.1	20	0.2012	1672.8	1.6803	0.1382	0.0786	79.520	0.474	1050	72	0	0	0	0	207	63
[36]	50.9	29.1	20	0.2012	1672.8	1.6803	0.1382	0.0786	79.520	0.474	1050	72	0	0	550	3	215	67
[36]	50.8	29.2	20	0.2011	1673.0	1.6800	0.1382	0.0786	79.509	0.474	1050	72	0	0	650	3	187	55
[36]	50.8	29.2	20	0.2011	1673.0	1.6800	0.1382	0.0786	79.509	0.474	1050	72	0	0	400	3	207	60
[36]	50.8	29.2	20	0.2011	1673.0	1.6800	0.1382	0.0786	79.509	0.474	1050	72	0	0	550	3	206	61
[36]	50.7	29.3	20	0.2010	1673.2	1.6796	0.1382	0.0786	79.499	0.474	1050	72	1050	3	0	0	58	41

[36]	50.7	29.3	20	0.2010	1673.2	1.6796	0.1382	0.0786	79.499	0.474	1050	72	0	0	550	3	192	49
[36]	50.7	29.3	20	0.2010	1673.2	1.6796	0.1382	0.0786	79.499	0.474	1050	72	0	0	0	0	195	52
[36]	50.7	29.3	20	0.2010	1673.2	1.6796	0.1382	0.0786	79.499	0.474	1050	72	0	0	400	3	199	54
[36]	50.7	29.3	20	0.2010	1673.2	1.6796	0.1382	0.0786	79.499	0.474	1050	72	0	0	650	3	195	55
[36]	50.6	29.4	20	0.2008	1673.4	1.6792	0.1383	0.0786	79.488	0.474	1050	72	0	0	550	3	191	29
[36]	50.6	29.4	20	0.2008	1673.4	1.6792	0.1383	0.0786	79.488	0.474	1050	72	0	0	400	3	174	29
[36]	50.6	29.4	20	0.2008	1673.4	1.6792	0.1383	0.0786	79.488	0.474	1050	72	1050	3	0	0	123	30
[36]	50.6	29.4	20	0.2008	1673.4	1.6792	0.1383	0.0786	79.488	0.474	1050	72	0	0	0	0	168	32
[36]	50.6	29.4	20	0.2008	1673.4	1.6792	0.1383	0.0786	79.488	0.474	1050	72	0	0	650	3	207	47
[36]	50.5	29.5	20	0.2007	1673.6	1.6789	0.1383	0.0786	79.477	0.474	1050	72	0	0	400	3	161	25
[36]	50.5	29.5	20	0.2007	1673.6	1.6789	0.1383	0.0786	79.477	0.474	1050	72	0	0	550	3	209	29
[36]	50.5	29.5	20	0.2007	1673.6	1.6789	0.1383	0.0786	79.477	0.474	1050	72	1050	3	0	0	164	29
[36]	50.5	29.5	20	0.2007	1673.6	1.6789	0.1383	0.0786	79.477	0.474	1050	72	0	0	0	0	167	32
[36]	50.5	29.5	20	0.2007	1673.6	1.6789	0.1383	0.0786	79.477	0.474	1050	72	0	0	650	3	218	36
[36]	50.4	29.6	20	0.2005	1673.8	1.6785	0.1383	0.0786	79.466	0.474	1050	72	0	0	550	3	238	27
[36]	50.4	29.6	20	0.2005	1673.8	1.6785	0.1383	0.0786	79.466	0.474	1050	72	1050	3	0	0	209	27
[36]	50.4	29.6	20	0.2005	1673.8	1.6785	0.1383	0.0786	79.466	0.474	1050	72	0	0	400	3	210	29
[36]	50.4	29.6	20	0.2005	1673.8	1.6785	0.1383	0.0786	79.466	0.474	1050	72	0	0	0	0	210	32
[36]	50.4	29.6	20	0.2005	1673.8	1.6785	0.1383	0.0786	79.466	0.474	1050	72	0	0	650	3	244	35
[36]	50.3	29.7	20	0.2004	1674.1	1.6781	0.1383	0.0786	79.455	0.475	1050	72	1050	3	0	0	234	30
[36]	50.2	29.8	20	0.2003	1674.3	1.6777	0.1384	0.0786	79.445	0.475	1050	72	0	0	400	3	264	29
[36]	50.2	29.8	20	0.2003	1674.3	1.6777	0.1384	0.0786	79.445	0.475	1050	72	0	0	650	3	267	35
[36]	50.2	29.8	20	0.2003	1674.3	1.6777	0.1384	0.0786	79.445	0.475	1050	72	0	0	0	0	268	36
[36]	50.2	29.8	20	0.2003	1674.3	1.6777	0.1384	0.0786	79.445	0.475	1050	72	0	0	550	3	280	37
[36]	50	30	20	0.2000	1674.7	1.6770	0.1384	0.0786	79.423	0.475	1050	72	1050	3	0	0	335	38
[36]	50	30	20	0.2000	1674.7	1.6770	0.1384	0.0786	79.423	0.475	1050	72	0	0	400	3	342	39
[36]	50	30	20	0.2000	1674.7	1.6770	0.1384	0.0786	79.423	0.475	1050	72	0	0	550	3	335	40
[36]	50	30	20	0.2000	1674.7	1.6770	0.1384	0.0786	79.423	0.475	1050	72	0	0	650	3	333	40

[36]	50	30	20	0.2000	1674.7	1.6770	0.1384	0.0786	79.423	0.475	1050	72	0	0	0	0	346	43
[16]	49	36	15	0.2139	1648.8	1.6853	0.1380	0.0782	72.785	0.460	950	1.5	1000	1	0	0	234	50
[27]	50.3	29.7	20	0.2004	1674.1	1.6781	0.1383	0.0786	79.455	0.475	1050	72	0	0	500	3	167	24
[27]	50.3	29.7	20	0.2004	1674.1	1.6781	0.1383	0.0786	79.455	0.475	1050	72	900	3	500	3	174	26
[27]	50.3	29.7	20	0.2004	1674.1	1.6781	0.1383	0.0786	79.455	0.475	1050	72	0	0	500	1	153	26
[27]	50.3	29.7	20	0.2004	1674.1	1.6781	0.1383	0.0786	79.455	0.475	1050	72	0	0	400	24	126	27
[27]	50.3	29.7	20	0.2004	1674.1	1.6781	0.1383	0.0786	79.455	0.475	1050	72	0	0	550	3	191	28
[27]	50.3	29.7	20	0.2004	1674.1	1.6781	0.1383	0.0786	79.455	0.475	1050	72	0	0	500	48	195	29
[27]	50.3	29.7	20	0.2004	1674.1	1.6781	0.1383	0.0786	79.455	0.475	1050	72	0	0	500	20	188	30
[27]	50.3	29.7	20	0.2004	1674.1	1.6781	0.1383	0.0786	79.455	0.475	1050	72	0	0	500	0.333	147	30
[27]	50.3	29.7	20	0.2004	1674.1	1.6781	0.1383	0.0786	79.455	0.475	1050	72	0	0	400	3	131	31
[27]	50.3	29.7	20	0.2004	1674.1	1.6781	0.1383	0.0786	79.455	0.475	1050	72	0	0	500	10	184	33
[27]	50.3	29.7	20	0.2004	1674.1	1.6781	0.1383	0.0786	79.455	0.475	1050	72	0	0	300	1	145	33
[27]	50.3	29.7	20	0.2004	1674.1	1.6781	0.1383	0.0786	79.455	0.475	1050	72	0	0	350	1	142	33
[27]	50.3	29.7	20	0.2004	1674.1	1.6781	0.1383	0.0786	79.455	0.475	1050	72	0	0	400	1	140	34
[27]	50.3	29.7	20	0.2004	1674.1	1.6781	0.1383	0.0786	79.455	0.475	1050	72	0	0	600	3	209	35
[27]	50.3	29.7	20	0.2004	1674.1	1.6781	0.1383	0.0786	79.455	0.475	1050	72	0	0	900	3	175	35
[27]	50.3	29.7	20	0.2004	1674.1	1.6781	0.1383	0.0786	79.455	0.475	1050	72	0	0	400	0.5	139	35
[27]	50.3	29.7	20	0.2004	1674.1	1.6781	0.1383	0.0786	79.455	0.475	1050	72	0	0	600	0.5	199	36
[27]	50.3	29.7	20	0.2004	1674.1	1.6781	0.1383	0.0786	79.455	0.475	1050	72	0	0	300	3	142	36
[27]	50.3	29.7	20	0.2004	1674.1	1.6781	0.1383	0.0786	79.455	0.475	1050	72	0	0	500	0.25	152	37
[27]	50.3	29.7	20	0.2004	1674.1	1.6781	0.1383	0.0786	79.455	0.475	1050	72	0	0	300	0.25	156	38
[27]	50.3	29.7	20	0.2004	1674.1	1.6781	0.1383	0.0786	79.455	0.475	1050	72	0	0	350	0.25	154	39
[27]	50.3	29.7	20	0.2004	1674.1	1.6781	0.1383	0.0786	79.455	0.475	1050	72	0	0	300	0.5	152	39
[27]	50.3	29.7	20	0.2004	1674.1	1.6781	0.1383	0.0786	79.455	0.475	1050	72	0	0	400	0.25	145	39
[27]	50.3	29.7	20	0.2004	1674.1	1.6781	0.1383	0.0786	79.455	0.475	1050	72	0	0	0	0	160	41
[27]	50.3	29.7	20	0.2004	1674.1	1.6781	0.1383	0.0786	79.455	0.475	1050	72	0	0	600	10	223	43
[27]	50.3	29.7	20	0.2004	1674.1	1.6781	0.1383	0.0786	79.455	0.475	1050	72	0	0	350	0.5	148	45

[27]	50.3	29.7	20	0.2004	1674.1	1.6781	0.1383	0.0786	79.455	0.475	1050	72	0	0	650	3	218	47
[27]	50.3	29.7	20	0.2004	1674.1	1.6781	0.1383	0.0786	79.455	0.475	1050	72	0	0	700	3	208	51
[40]	50.3	34.7	15	0.2158	1646.0	1.6901	0.1377	0.0782	72.926	0.458	1050	72	900	1	550	3	103	55
[40]	50.3	34.7	15	0.2158	1646.0	1.6901	0.1377	0.0782	72.926	0.458	1050	72	900	1	450	10	37	55
[40]	50.3	34.7	15	0.2158	1646.0	1.6901	0.1377	0.0782	72.926	0.458	1050	72	900	1	500	3	68	56
[40]	50.3	34.7	15	0.2158	1646.0	1.6901	0.1377	0.0782	72.926	0.458	1050	72	900	1	600	10	170	57

*Table 0.3. Second Dataset**

Ref.	**Ni [at.%]**	**Ti [at.%]**	**Hf [at.%]**	**Cv**	**Calculated melting point* [℃]**	**Calculated electro-negativity***	**Calculated atomic radius* [nm]**	**Calculated ionic radius* [nm]**	**Calculated atomic mass* [amu]**	**Calculated Waber-Cromer's pseudo-potential radius* [Å]**	**A_f [℃]**	**Thermal hysteresis [℃]**
[17]	51	49	0	0.281724	15.6035	1.7287	0.13578	0.07702	53.4131	0.40536	2	22
[35]	51	36.5	12.5	0.225487	16.30475	1.6987	0.13728	0.07802	69.73685	0.44786	49	66
[17]	51	29	20	0.201369	16.7255	1.6807	0.13818	0.07862	79.5311	0.47336	53	49
[17]	51	19	30	0.176236	17.2865	1.6567	0.13938	0.07942	92.5901	0.50736	522	129
[24]	50.8	29.2	20	0.201096	16.7298	1.67996	0.138224	0.078616	79.50948	0.473688	110	33
[17]	50.7	49.3	0	0.281208	15.60995	1.72759	0.135846	0.077014	53.38067	0.405852	34	28
[17]	50.7	44.3	5	0.255682	15.89045	1.71559	0.136446	0.077414	59.91017	0.422852	49	58
[17]	50.7	39.3	10	0.234405	16.17095	1.70359	0.137046	0.077814	66.43967	0.439852	45	110
[17]	50.7	34.3	15	0.216397	16.45145	1.69159	0.137646	0.078214	72.96917	0.456852	76	50
[17]	50.7	29.3	20	0.200959	16.73195	1.67959	0.138246	0.078614	79.49867	0.473852	171	28
[17]	50.7	24.3	25	0.187577	17.01245	1.66759	0.138846	0.079014	86.02817	0.490852	333	72
[17]	50.7	19.3	30	0.175865	17.29295	1.65559	0.139446	0.079414	92.55767	0.507852	620	181
[17]	50.6	29.4	20	0.200822	16.7341	1.67922	0.138268	0.078612	79.48786	0.474016	174	53
[11]	50.6	24.4	25	0.187447	17.0146	1.66722	0.138868	0.079012	86.01736	0.491016	356	66
[4]	50.5	36.2	13.3	0.221907	16.36038	1.69493	0.137486	0.078074	70.72752	0.4514	31.2	62.9

[20]	50.5	34.5	15	0.216108	16.45575	1.69085	0.13769	0.07821	72.94755	0.45718	88	36.2
[36]	50.5	29.5	20	0.200685	16.73625	1.67885	0.13829	0.07861	79.47705	0.47418	209	29
[36]	50.4	29.6	20	0.200548	16.7384	1.67848	0.138312	0.078608	79.46624	0.474344	210	32
[17]	50.3	49.7	0	0.280518	15.61855	1.72611	0.135934	0.077006	53.33743	0.406508	78	32
[17]	50.3	44.7	5	0.255033	15.89905	1.71411	0.136534	0.077406	59.86693	0.423508	103	62
[17]	50.3	39.7	10	0.233793	16.17955	1.70211	0.137134	0.077806	66.39643	0.440508	127	75
[40]	50.3	34.7	15	0.215819	16.46005	1.69011	0.137734	0.078206	72.92593	0.457508	170	57
[27]	50.3	29.7	20	0.200411	16.74055	1.67811	0.138334	0.078606	79.45543	0.474508	223	43
[4]	50.3	25	24.7	0.187808	17.00422	1.66683	0.138898	0.078982	85.59316	0.490488	422	82
[17]	50.3	24.7	25	0.187057	17.02105	1.66611	0.138934	0.079006	85.98493	0.491508	428	95
[17]	50.3	19.7	30	0.175371	17.30155	1.65411	0.139534	0.079406	92.51443	0.508508	622	135
[36]	50.2	29.8	20	0.200274	16.7427	1.67774	0.138356	0.078604	79.44462	0.474672	268	36
[17]	50	50	0	0.28	15.625	1.725	0.136	0.077	53.305	0.407	106	37
[17]	50	45	5	0.254545	15.9055	1.713	0.1366	0.0774	59.8345	0.424	141	54
[22]	50	42	8	0.241379	16.0738	1.7058	0.13696	0.07764	63.7522	0.4342	115	69.42
[34]	50	40	10	0.233333	16.186	1.701	0.1372	0.0778	66.364	0.441	187	71
[22]	50	39	11	0.229508	16.2421	1.6986	0.13732	0.07788	67.6699	0.4444	154.45	60.9
[12]	50	38	12	0.225806	16.2982	1.6962	0.13744	0.07796	68.9758	0.4478	194	52
[22]	50	36	14	0.21875	16.4104	1.6914	0.13768	0.07812	71.5876	0.4546	188.1	56.12
[17]	50	35	15	0.215385	16.4665	1.689	0.1378	0.0782	72.8935	0.458	249	45
[22]	50	33	17	0.208955	16.5787	1.6842	0.13804	0.07836	75.5053	0.4648	224.31	44.53
[37]	50	30	20	0.2	16.747	1.677	0.1384	0.0786	79.423	0.475	331	45
[17]	50	25	25	0.186667	17.0275	1.665	0.139	0.079	85.9525	0.492	426	48
[17]	50	20	30	0.175	17.308	1.653	0.1396	0.0794	92.482	0.509	583	66
[17]	49.8	50.2	0	0.279654	15.6293	1.72426	0.136044	0.076996	53.28338	0.407328	115.3	32
[3]	49.8	48.2	2	0.268893	15.7415	1.71946	0.136284	0.077156	55.89518	0.414128	121.7	39.1
[3]	49.8	46.2	4	0.25893	15.8537	1.71466	0.136524	0.077316	58.50698	0.420928	133.8	48
[17]	49.8	45.2	5	0.25422	15.9098	1.71226	0.136644	0.077396	59.81288	0.424328	137.6	58

[3]	49.8	44.2	6	0.249678	15.9659	1.70986	0.136764	0.077476	61.11878	0.427728	148.4	57.5
[29]	49.8	42.2	8	0.241065	16.0781	1.70506	0.137004	0.077636	63.73058	0.434528	142	73
[29]	49.8	40.7	9.5	0.234986	16.16225	1.70146	0.137184	0.077756	65.68943	0.439628	159	69
[17]	49.8	40.2	10	0.233027	16.1903	1.70026	0.137244	0.077796	66.34238	0.441328	188	62
[29]	49.8	39.2	11	0.229205	16.2464	1.69786	0.137364	0.077876	67.64828	0.444728	182	59
[3]	49.8	35.2	15	0.215095	16.4708	1.68826	0.137844	0.078196	72.87188	0.458328	257.9	50.9
[19]	49.8	30.2	20	0.199726	16.7513	1.67626	0.138444	0.078596	79.40138	0.475328	331	46.4
[17]	49.8	25.2	25	0.186406	17.0318	1.66426	0.139044	0.078996	85.93088	0.492328	442	36
[17]	49.8	20.2	30	0.174752	17.3123	1.65226	0.139644	0.079396	92.46038	0.509328	579	62
[39]	49.5	35.5	15	0.21466	16.47725	1.68715	0.13791	0.07819	72.83945	0.45882	254.8	49.3
[23]	49.42	35.95	14.63	0.215773	16.45821	1.687742	0.137883	0.078159	72.34762	0.457693	230	54
[44]	49.4	38.6	12	0.224906	16.3111	1.69398	0.137572	0.077948	68.91094	0.448784	247	62
[42]	49	48	3	0.262481	15.8148	1.7141	0.13658	0.07722	57.1146	0.41884	128	52
[42]	49	46	5	0.252915	15.927	1.7093	0.13682	0.07738	59.7264	0.42564	142	62
[42]	49	44	7	0.244023	16.0392	1.7045	0.13706	0.07754	62.3382	0.43244	167	76
[34]	49	41	10	0.231797	16.2075	1.6973	0.13742	0.07778	66.2559	0.44264	194	64
[16]	49	36	15	0.213933	16.488	1.6853	0.13802	0.07818	72.7854	0.45964	234	50
[5]	48.5	36.5	15	0.213206	16.49875	1.68345	0.13813	0.07817	72.73135	0.46046	255	55
[38]	40	50	10	0.217687	16.401	1.664	0.1394	0.0776	65.283	0.4574	205	65
[38]	35	50	15	0.193038	16.789	1.6335	0.1411	0.0779	71.272	0.4826	290	55
[32]	27	70	3	0.223726	16.2878	1.6327	0.14142	0.07678	54.7364	0.45492	132.4	93.2
[32]	24	70	6	0.205749	16.5206	1.6144	0.14244	0.07696	58.3298	0.47004	164.6	100
[32]	21	70	9	0.189481	16.7534	1.5961	0.14346	0.07714	61.9232	0.48516	254.7	78.9

* : Reference numbers refers to references provided in Section 2